

1  
2  
3  
4  
5  
6  
7  
8  
9  
10  
11  
12  
13  
14  
15  
16  
17  
18  
19  
20  
21  
22  
23  
24  
25  
26  
27  
28  
29  
30  
31  
32  
33  
34  
35  
36  
37  
38  
39  
40

# Spatio-temporal diversity and genetic architecture of pyrantel resistance in *Cylicocyclus nassatus*, the most abundant horse parasite

Guillaume Sallé<sup>1,\*</sup>, Élise Courtot<sup>1</sup>, Cédric Cabau<sup>2</sup>, Hugues Parrinello<sup>3</sup>, Delphine Serreau<sup>1</sup>, Fabrice Reigner<sup>4</sup>, Amandine Gesbert<sup>4</sup>, Lauriane Jacquinet<sup>1</sup>, Océane Lenhof<sup>1</sup>, Annabelle Aimé<sup>5</sup>, Valérie Picandet<sup>5</sup>, Tetiana Kuzmina<sup>6,7</sup>, Oleksandr Holovachov<sup>8</sup>, Jennifer Bellaw<sup>9</sup>, Martin K. Nielsen<sup>9</sup>, Georg von Samson-Himmelstjerna<sup>10</sup>, Sophie Valière<sup>11</sup>, Marie Gislard<sup>11</sup>, Jérôme Lluch<sup>11</sup>, Claire Kuchly<sup>11</sup>, Christophe Klopp<sup>12</sup>

1, Université de Tours, INRAE UMR1282 Infectiologie et Santé Publique, Nouzilly - France  
2, Sigénae, GenPhySE, Université de Toulouse, INRAE, ENVT, Castanet Tolosan - France  
3, MGX-Montpellier GenomiX, Univ. Montpellier, CNRS, INSERM, Montpellier - France  
4, INRAE UE 1297 Unité Expérimentale de Physiologie Animale de l'Orfrasière, Nouzilly - France  
5, Centre hospitalier vétérinaire équin de St Michel de Livet, Cour Samson, Livarot-Pays-d'Auge - France  
6, I. I. Schmalhausen Institute of Zoology NAS of Ukraine, Kyiv - Ukraine.  
7, Institute of Parasitology, Slovak Academy of Sciences, Košice - Slovak Republic.  
8, Department of Zoology, Swedish Museum of Natural History, Stockholm - Sweden  
9, M.H. Gluck Equine Research Center, Department of Veterinary Science, University of Kentucky, Lexington (KY) - USA  
10, Institute for Parasitology and Tropical Veterinary Medicine, Freie Universitaet Berlin, Robert-von-Ostertag-Str. 7, Berlin - Germany  
11, INRAE, US 1426, GeT-PlaGe, Genotoul, France Génomique, Université Fédérale de Toulouse, Castanet Tolosan - France  
12, Sigénae, Genotoul Bioinfo, MIAT UR875, INRAE, Castanet Tolosan - France

\*Corresponding author  
Correspondence: [gsalle.inra.email@gmail.com](mailto:gsalle.inra.email@gmail.com)

## ABSTRACT

Cyathostomins are a complex of 50 intestinal parasite species infecting horses and wild equids. The massive administration of modern anthelmintic drugs has increased their relative abundance in horse helminth communities and selected drug-resistant isolates worldwide. *Cylicocyclus nassatus* is the most prevalent and the most abundant species. The tedious identification and isolation of these worms have hampered studies of their biology that remain largely uncharacterised. Here we have leveraged ultra-low input sequencing protocols to build a

Deleted: has

42 reference genome for the most prevalent horse strongyle species. Using this resource, we have  
43 established the first estimates of its genetic diversity and population structure on a gradient  
44 ranging from Ukraine (close to modern horse domestication area) to North America, while  
45 capturing a 19th-century snapshot of *C. nassatus* diversity in Egypt. Our results support a diverse  
46 and lowly structured global population. Modern populations displayed lower nucleotide diversity  
47 relative to the old North African isolate. We identified the first genetic candidates upon which  
48 pyrantel (an anthelmintic drug used in companion animals) selection likely applied in field  
49 populations, highlighting previously suspected genes coding for nicotinic acetylcholine receptor  
50 subunits, and identifying new candidates showing differential expression in independently  
51 evolved *C. elegans* lines. These results offer a first resource to widen current knowledge on  
52 cyathostomin biology, unravel novel aspects of pyrantel resistance mechanisms and provide  
53 candidate genes to track pyrantel resistance in the field.

54  
55 **Keywords:** nematode, horse, cyathostomin, drug resistance, pyrantel, *Caenorhabditis elegans*  
56

Deleted: 19XIX<sup>th</sup> century

Deleted: and a significant reducclos of genetic diversity in modern populations over the last century

Deleted: -

Deleted: -

Deleted: applies

## Introduction

Parasitic nematodes account for 11.8 million disability-adjusted life years in humans (G. B. D. DALYs and Hale Collaborators 2017) and inflict major losses on pet and livestock species (Kaplan and Vidyashankar 2012; von Samson-Himmelstjerna et al. 2021; Nielsen 2022; Marsh and Lakritz 2023). While prevention and sanitation have played a major role in bringing the Guinea worm to the brink of extinction (Durrant et al. 2020), parasite control programs still heavily rely on the administration of anthelmintic drugs in both the medical (Bradley et al. 2021; Gandasegui et al. 2022) and veterinary settings (Laing et al. 2017; von Samson-Himmelstjerna et al. 2021; Nielsen 2022; Marsh and Lakritz 2023). In livestock-infecting species, anthelmintic treatments have reduced nematode diversity at both the species and community levels and species scales as illustrated in horses. In this rich host-parasite system, the once predominant horse large strongyles (*Strongylus* spp.) are now encountered at low prevalence across managed horse populations (Jürgenschellert et al. 2022) while they dominate parasite communities in a Canadian feral horse population (Jenkins et al. 2020). Field observations also support increased odds to encounter *S. vulgaris* on farms implementing evidence-based treatments (Tydén et al. 2019). On the contrary, cyathostomins, a complex of forty described species inhabiting the horse hindgut and dominated by *Cylicocyclus nassatus* (Ogbourne 1972; Lyons et al. 1992; Bucknell et al. 1995; Collobert-Laugier et al. 2002; Kuzmina et al. 2016), have become predominant (Herd 1990) and represent the most important cause of parasite-mediated death in young horses (Sallé et al. 2020). Cyathostomins are encountered worldwide across a wide range of equids, including donkeys, horses, and zebras (Lichtenfels et al. 2008; Kuzmina and Kuzmin 2008; Kuzmina et al., 2013; Tombak et al. 2021). However, investigation of their biology has been hampered by the complexity of their assemblages which usually encompass more than ten species within a horse, and the tediousness of their morphological identification (Bellaw and Nielsen, 2020; Lichtenfels et al. 2008). Recent applications of metabarcoding experiments (Poissant et al. 2021) have uncovered additional aspects of their response to drugs (Nielsen et al. 2022) and plant products (Malsa et al. 2022), their interaction with their host gut microbiota (Boisseau et al. 2023) or fluctuation in their relative abundance throughout a grazing season in unmanaged horses (Sargison et al. 2022). However, the genetics of drug resistance in cyathostomins remains unknown for drugs other than benzimidazoles (Hodgkinson et al. 2008). Beyond reshaping helminth community structure, anthelmintic drugs have also remodelled the genetic diversity of parasite species as evidenced in *Haemonchus contortus* (Doyle et al. 2019; Sallé et al. 2019; Doyle, Laing, et al. 2022), a blood-feeding parasite of small-ruminants. In that case, a drastic loss of genetic diversity occurred over a beta-tubulin coding gene in benzimidazole-resistant isolates (Sallé et al. 2019). Additional efforts of breeding experimental back-cross lines have also shed light on the molecular architecture of resistance to levamisole (Doyle, Laing, et al. 2022), ultimately yielding genetic markers to anticipate the selection of resistant isolates in the field (Antonopoulos et al. 2022). Altogether, the role of candidate genes already proposed to affect anthelmintic sensitivity to benzimidazoles (Kwa et al. 1995) or levamisole (Neveu et al. 2010) have been confirmed using genome-wide mapping approaches, but discrepancies have emerged for the genetic structure of ivermectin resistance (Laing et al. 2022). In addition, the genes associated with the resistance to other drugs like pyrantel remain poorly characterised. Pyrantel is a widely used anthelmintic drug for parasite control in humans (Moser et al. 2017), pets (Kopp et al. 2008), and horses (Lyons et al. 1999). Reduced pyrantel efficacy has been observed in the dog hookworm *Ancylostoma caninum* and frequently occurs in the horse cyathostomins (Lyons 2003; Sallé et al. 2017). Early electrophysiology measures in muscle vesicles of the pig parasites *Oesophagostomum dentatum* (Robertson et al. 1994) or *Ascaris suum* (Robertson et al. 2000) concluded that pyrantel acts as an acetylcholine agonist on cation channels present at neuromuscular junctions. This ultimately results in their spastic paralysis and elimination from their host. The knock-down of the genes coding for some of these receptor subunits affected *C. elegans* susceptibility towards pyrantel, either completely for *unc-29* and *unc-63* knock-outs or partially for *unc-38* knock-outs (Sleigh 2010). In addition, pyrantel-resistant *A. caninum* isolated from dogs had reduced expression of these genes in comparison to a susceptible isolate (Kopp et al. 2009). Other heterologous expression experiments of *H. contortus* *acr-8* (Blanchard et al. 2018) or *acr-26* and *acr-27* (*H. contortus* and

Deleted: to

Deleted: Von

Deleted: on

Deleted: Von

Deleted: s

Formatted: Font: Italic

Formatted: Font: Italic

Deleted: -

Formatted: Font: Italic

Deleted: -

Deleted: or

Deleted: that

Deleted: But

Formatted: Font: Italic

Deleted: blood

Formatted: Font: Italic

Formatted: Font: Italic

Formatted: Font: Italic

Deleted: was

Deleted: ing

Formatted: Font: Italic

126 *Parascaris* sp.) in *C. elegans* also increased the resistance level to this drug (Courtot et al. 2015). Despite these  
 127 converging strands of evidence, it is yet unknown whether pyrantel treatment in the field primarily selects  
 128 variants of these candidates, whether additional candidates contribute to decreased pyrantel sensitivity, and  
 129 if the known targets shared by *C. elegans* and *A. caninum* are under selection in cyathostomin populations.  
 130 To bridge this knowledge gap, this study aims to investigate the genetic architecture of pyrantel resistance in  
 131 cyathostomin populations using a set of pyrantel-sensitive and -resistant isolates. The success of mapping  
 132 approaches to isolate drug resistance candidates has relied on well-annotated chromosome-level assemblies.  
 133 While a substantial number of assemblies have recently been produced for helminth species of medical and  
 134 veterinary importance (International Helminth Genomes 2019), genome assembly has proved challenging for  
 135 parasitic nematodes due to the limited genetic material available for each individual and their highly  
 136 heterozygous and repetitive medium-sized genomes (International Helminth Genomes 2019; Doyle 2022). In  
 137 some cases like the horse cyathostomins, the complexity of collecting, isolation, and identification of worm  
 138 material from horses (Louro et al. 2021) adds additional challenges to produce sufficient quantities of good  
 139 quality DNA and RNA. To date, *Cylicostephanus goldi* is the only cyathostomin species with a released genome  
 140 (International Helminth Genomes 2019) and transcriptome (Cwiklinski et al. 2013) assemblies. However, short-  
 141 read data generated for this species could not resolve the full genome sequence and yielded a heavily  
 142 fragmented assembly (International Helminth Genomes 2019). Nonetheless, the recent description of ultra-  
 143 low input protocol applicable to long-read sequencing technologies (Kingan et al. 2019) opens new  
 144 perspectives for the generation of high-quality genome assemblies and subsequent study of genetic diversity  
 145 for hard-to-collect species.  
 146 Using this approach and Hi-C genomic analysis technique, we have built a chromosomal assembly from a single  
 147 *Cylicocyclus nassatus* individual and applied Hi-C technology to scaffold a chromosome-level genome. We  
 148 investigated the diversity of this species using contemporary worms covering an East-West gradient from  
 149 Ukraine to Kentucky, USA, and established patterns of variation between these contemporary populations and  
 150 an old isolate collected in Egypt in the 19<sup>th</sup> century. Finally, a comparison of the genetic diversity of pyrantel-  
 151 resistant and -susceptible isolates identified novel candidates for pyrantel resistance in *C. nassatus*. Orthologs  
 152 of these candidate genes were found differentially expressed in evolved *C. elegans* lines.  
 153  
 154  
 155  
 156  
 157

- Formatted: Font: Italic
- Formatted: Font: Italic
- Formatted: Font: Italic
- Formatted: Font: Italic
- Deleted: telomere-to-telomere
- Deleted: to collect
- Deleted: isolate
- Deleted: identify
- Deleted: Lichtenfels et al. 2008
- Formatted: Font: Italic
- Formatted: Font: Italic
- Deleted: telomere-to-telomere
- Deleted: the
- Deleted: XIX
- Deleted:
- Deleted: that species
- Deleted: that
- Formatted: Font: Italic

## Material and methods

### Worm collection procedures

Unless stated otherwise, worms were harvested from Welsh ponies maintained in INRAE facilities. Infected ponies were given pyrantel pamoate (6.6 mg/kg live-weight, Strongid<sup>®</sup>, Zoetis, Malakoff, France) per os and faecal matter was harvested between 18 h and 24 h after treatment to collect individual male worms. Upon collection, worms were bathed in PBS 1x to remove faecal debris, and placed in microcentrifuge tubes left on ice for no more than 15 min before being put at -80°C. For Hi-C data production, 70 worms were used and collected following the same procedure. In that case, however, worms had their head cut for genotyping while their body was flash frozen.

Transcriptomic data were generated from whole worms. These worms were picked from faecal matter collected 18 h after pyrantel treatment, briefly bathed in 1x PBS, placed in a microcentrifuge tube, and flash frozen in liquid nitrogen.

To quantify the sex ratio in cyathostomins released after pyrantel treatment, the faecal matter of 10 Welsh ponies was collected between 15 h and 24 h after drug administration. On every occasion, the worms of each sex were counted from 200 g of faeces.

### DNA and RNA extraction protocols for genome assembly and annotation

DNA was extracted following a salting-out procedure to reduce the number of processing steps. Worms were gently crushed with a sterile pestle and incubated for 3 hours at 56°C in a lysis buffer adapted from a previous experiment on mosquitoes (Kingan et al. 2019). Following incubation, NaCl was added to the mix before precipitation was induced with isopropanol. After centrifugation (6250g at 4°C for 5 min), the DNA pellet was washed with 70% ethanol and resuspended in 30 µL of TE buffer. A second DNA library was produced using 2.5 µL native DNA from the same sample after the whole genome amplification procedure following the REPLI-G<sup>®</sup> (Qiagen) manufacturer's recommendation.

Genome annotation was based on RNAseq data from male and female *C. nassatus*. To isolate *C. nassatus* from other cyathostomin species after worm collection, simultaneous DNA and RNA extraction (AllPrep<sup>®</sup> DNA/RNA mini kit, Qiagen) was performed on 94 worms. DNAs were used for Sanger sequencing of the ITS-2 and COI regions to subsequently isolate *C. nassatus* species. RNAs were stored at -80°C before three pools of four to five males and three pools of three to four females were made for sequencing.

### PacBio sequencing of a single *C. nassatus* worm

The REPLI-g amplified and non-amplified native DNA left from the same single male worm were subsequently processed at GeT-PlaGe core facility (INRAe Toulouse) to prepare two libraries according to the manufacturer's instructions "Procedure & Checklist - Preparing HiFi Libraries from Low DNA Input Using SMRTbell<sup>®</sup> Express Template Prep Kit 2.0". At each step, DNA was quantified using the Qubit dsDNA HS Assay Kit (Life Technologies). DNA purity was tested using a nanodrop (ThermoFisher) and size distribution and degradation were assessed using the Femto pulse Genomic DNA 165 kb Kit (Agilent). Purification steps were performed using AMPure PB beads (PacBio) and 1 µg of DNA was purified and then sheared at 13 kb using the Megaruptor1 system (Diagenode). The library was size-selected, using AMPure<sup>®</sup> PB beads (Pacbio) to remove less than 3kb-long templates. Using Binding kit 2.0 (primer V4, polymerase 2.0) and sequencing kit 2.0, the 12 kb library was sequenced onto 1 SMRTcell on Sequel2 instrument at 40 pM with a 2-hour pre-extension and a 30-hour movie. A second library was prepared from the same DNA sample following the manufacturer's instructions "Procedure & Checklist - Preparing HiFi SMRTbell<sup>®</sup> Libraries from Ultra-Low DNA Input". At each step, DNA was quantified using the Qubit dsDNA HS Assay Kit (Life Technologies). DNA purity was tested using the nanodrop (ThermoFisher) and size distribution and degradation assessed using the Femto pulse Genomic DNA 165 kb Kit (Agilent). Purification steps were performed using AMPure PB beads (PacBio). 13 ng of DNA was purified then sheared at 10 kb using the Megaruptor1 system (Diagenode). Using SMRTbell<sup>®</sup> gDNA Sample Amplification Kit, 5ng of DNA was amplified by 2 complementary PCR reactions (13 cycles). Then 500 ng of the library was size-selected, using a 6.5 kb cutoff on the BluePippin Size Selection system (Sage Science) with the "0.75% DF Marker S1 3-10 kb Improved Recovery" protocol. Using Binding kit 2.0 (primer V4, polymerase 2.0) and

Deleted: liveweight

Deleted: x

Formatted: Superscript

Deleted: x

Deleted: -

Formatted: Font: Italic

Formatted: Font: Italic

Formatted: Font: Italic

Deleted: native

Deleted: sample extracted from a

Deleted: was

Deleted: 3kb

Deleted: 2

Deleted: s

Deleted: 30

Deleted: s

Deleted: DNA

232 sequencing kit 2.0, the 9.5 kb library was sequenced onto one SMRTcell on Sequel2 instrument at 50 pM with  
233 a 2-hour pre-extension and a 30-hour movie. The low- and ultra-low input protocols yielded 6 and 26 Gbp  
234 respectively, corresponding to 615,427 and 2,780,682 CSS reads respectively and 10× and 44× depth of  
235 coverage.

Deleted: 2

Deleted: s

Deleted: 30

Deleted: s

Deleted: x

Deleted: were

Deleted: were

Deleted: double

Deleted: x

### 237 RNA sequencing of male and female *C. nassatus* worms

238 RNAseq was performed at the GeT-PlaGe core facility, INRAe Toulouse. RNA-seq libraries have been prepared  
239 according to Illumina's protocols using the Illumina TruSeq Stranded mRNA sample prep kit to analyse mRNA.  
240 Briefly, mRNA was selected using poly-T beads. Then, RNA was fragmented to generate double-stranded cDNA  
241 and adaptors were ligated to be sequenced. 11 cycles of PCR were applied to amplify libraries. Library quality  
242 was assessed using a Fragment Analyser and libraries were quantified by QPCR using the Kapa Library  
243 Quantification Kit. RNA-seq experiments have been performed on an Illumina NovaSeq 6000 using a paired-  
244 end read length of 2×150 pb with the associated sequencing kits.

### 246 Hi-C library preparation and sequencing

247 Hi-C library was constructed using the Arima-HiC kit (Arima, ref. A510008) and the Accel NGS 2S Plus DNA  
248 Library Kit (Swift Biosciences, ref. SW21024). Briefly, we pulverised complete worms in liquid nitrogen using a  
249 mortar and crosslinked the pulverised tissue using a 2% formaldehyde solution. After tissue lysis, we digested  
250 the crosslinked DNA according to the manufacturer's protocol. We repaired the digested DNA using  
251 biotinylated nucleotides and performed a ligation aiming for spatially proximal digested ends of DNA. We  
252 purified the proximally ligated DNA, sonicated it using an e220 focused-ultrasonicator (Covaris), and enriched  
253 the biotinylated fragments. Starting from enriched biotinylated fragments, we constructed an NGS library using  
254 the Accel-NGS 2S Plus DNA library kit (Swift Biosciences, SW21024) according to ARIMA's instruction, whereby  
255 fragments were first end-repaired before indexed adapters ligation. After purification, a small fraction of the  
256 indexed DNA was used to determine by qPCR the number of PCR cycles necessary for optimal amplification.  
257 Based on this result, we performed 6 cycles of PCR amplification on the remaining indexed DNA. The size  
258 distribution of the resulting library was monitored using a Fragment Analyzer with the High Sensitivity NGS kit  
259 (Agilent Technologies, Santa Clara, CA, USA) and the library was quantified using microfluorimetry (Qubit  
260 dsDNA HS kit, ThermoFischer scientific). The library was denatured with NaOH, neutralised with Tris-HCl, and  
261 diluted to 300 pM. Clustering and sequencing were performed on a NovaSeq 6000 (Illumina, San Diego, CA,  
262 USA) using the paired end 150 nt protocol on 1 lane of a flow cell SP. Image analyses and base calling were  
263 performed using the Miniseq Control Software and the Real-Time Analysis component (Illumina).  
264 Demultiplexing was performed using Illumina's conversion software (bcl2fastq 2.20.0.422). The quality of the  
265 raw data was assessed using FastQC v0.11.9 (<http://www.bioinformatics.babraham.ac.uk/projects/fastqc/>)  
266 from the Babraham Institute and the Illumina software SAV (Sequencing Analysis Viewer). FastqScreen  
267 ([Wingett and Andrews 2018](#)) was used to identify potential contamination.

Deleted: a

### 269 Genome assembly, gene model prediction, and annotation

270 HiFi data (30 Gb) were adapter-trimmed and filtered for low-quality reads. Genome assembly graphs were  
271 produced using HiFiasm ([Cheng et al. 2021](#)) v0.16.1 using default parameters. Assembly completeness was  
272 assessed using BUSCO ([Seppey et al. 2019](#)) v 5.2.2 (nematoda\_odb10 gene set, n = 3,331), and metrics were  
273 estimated using Quast v-5.0.2 ([Gurevich et al. 2013](#)).  
274 This first assembly was subsequently used as a back-bone for scaffolding with Hi-C data. These data were  
275 processed with the juicer pipeline ([Durand, Shamim, et al. 2016](#)) v 1.5.7. The assembly was scaffolded with 3d-  
276 DNA ([Dudchenko et al. 2017](#)) and manually corrected with juicebox ([Durand, Robinson, et al. 2016](#)) (version  
277 1.11.08).  
278 The mitochondrial genome was assembled using the mitoHiFi v2.2 software ([Uliano-Silva et al. 2022](#)), feeding  
279 quality filtered HiFi reads, and the *C. nassatus* reference mitogenome ([Gao et al. 2017](#)) as a backbone. The final  
280 mitogenome sequence was subsequently added to the assembly fasta file. We also identified and removed the

Deleted: dna

Formatted: Font: Italic

292 chimeric hifiasm assembled mitochondrion sequence (38 Kbp in length, matched to scaffold 57 with the  
 293 minimap2 software (Li 2018).  
 294 Repeat elements were identified using RepeatMasker (Tarailo-Graovac and Chen 2009) v4.0.7, Dust (Morgulis  
 295 et al. 2006) v1.0.0 and TRF (Benson 1999) v4.09. To locate repeat regions, the *C. elegans* libraries and a *C.*  
 296 *nassatus*-specific de novo repeat library built with RepeatModeler (Flynn et al. 2020) v1.0.11 were fed to  
 297 RepeatMasker (Tarailo-Graovac and Chen 2009). Bedtools v2.26.0 was used to aggregate repeated regions  
 298 identified with the three tools and to soft mask the genome.  
 299 Gene models were built from RNAseq data generated from male and female samples. RNAseq reads were  
 300 mapped onto the masked genome (repeatMasker v4.0.7) using the HiSat2 (Zhang et al. 2021) software to  
 301 produce hints subsequently used for protein-to-genome alignment with exonerate. Ab initio gene structures  
 302 were subsequently estimated with the BRAKER (Hoff et al. 2019) pipeline relying on both RNAseq data and  
 303 available proteomes for other clade V species (*Ancylostoma ceylanicum*, *Haemonchus contortus*,  
 304 *Caenorhabditis elegans*, *C. inopinata*, *C. remanei*, *C. tropicalis*) and more phylogenetically distant species  
 305 (*Brugia malayi* and *Onchocerca volvulus*) for clade III, and *Trichuris muris* for clade I parasitic nematodes. These  
 306 gene predictions were fed to MAKER (Campbell et al. 2014) for final gene model prediction. Gene annotation  
 307 was achieved with the EnTAP software (Hart et al. 2020) to assign homology information from the EggNOG  
 308 (Hernández-Plaza et al. 2023) database and protein domain from PFAM (Mistry et al. 2021) and InterPro  
 309 (Paysan-Lafosse et al. 2023) databases.

### 311 Comparative genomic analyses

312 The synteny between the *C. nassatus* and *H. contortus* genomes was inferred after aligning both references  
 313 against one another, using the PROMER software (Delcher et al. 2002) with the -mum option to recover the  
 314 only exact matches being unique between the query and reference sequences. Hits were subsequently filtered  
 315 with the delta-filter tool, setting the minimal length of a match at 500 amino acids. A custom perl script (Cotton  
 316 et al. 2017) was subsequently used to draw the circus plot, showing links with 70% similarity and a minimal  
 317 length of 10 Kbp. Ortholog groups were identified using the Orthofinder software v2.5.4 (Emms and Kelly 2019),  
 318 considering the subset of the most complete nematode genomes (N50 above 10 Mbp) present in  
 319 WormBaseParasite v.17 and annotated with RNAseq data, including clade V parasitic (*H. contortus*) and free-  
 320 living species (*Caenorhabditis elegans*, *C. briggsae*, *C. inopinata*, *C. nigoni*, *C. remanei*, *C. tropicalis*, and  
 321 *Pristionchus pacificus*), clade IV plant (*Bursaphelenchus xylophilus*, *Heterodera glycines*) and animal parasites  
 322 (*Strongyloides ratti*), filarial nematodes (*Brugia malayi*, *Onchocerca volvulus*) and *Trichuris muris* as a clade I  
 323 representative. Because of the close phylogenetic relationship with the family Ancylostomatidae, the  
 324 *Ancylostoma ceylanicum* proteome was also considered. The species tree was built using the iTOL software  
 325 (Letunic and Bork 2021). Gene family evolution was performed with the CAFE v3 software (Han et al. 2013).

### 327 Differential transcriptomic response of male and female *C. nassatus* after exposure to pyrantel

328 RNA-seq reads were mapped with the Salmon software v1.4 (Patro et al. 2017) with correction for GC-content,  
 329 sequence-specific and position biases and the validateMappings option. Pseudo-counts were imported with  
 330 the tximport package v1.18.0 and differential gene expression was estimated with the DESeq2 v1.30.1 package  
 331 (Love et al. 2014). Out of the 22,568 expressed genes, 12,569 with at least ten counts in five replicates were  
 332 considered for analysis. Female worm gene counts displayed a bimodal distribution. The cut-off splitting the  
 333 two underlying distributions was determined with the peakPick package v0.11. Differential gene expression  
 334 was applied to both gene populations, i.e. those with a median count below or above the identified cut-off. In  
 335 any case, genes showing an absolute fold change above 2 and an adjusted P-value below 1% were deemed  
 336 significant.

337 Gene Ontology enrichment was run using the topGO package v2.42 (Alexa 2016) and processed with the  
 338 GeneTonic package (Marini et al. 2021). GO terms with a P-value below 1% were considered significant. To gain  
 339 additional functional insights, one-to-one orthologs of the differentially expressed genes in *C. elegans* were  
 340 considered for tissue or phenotype enrichment using the wormbase enrichment tool (considering a q-value  
 341 cut-off of 1%). To investigate differences between male and female worms that would not be associated with

Formatted: Font: Italic

Formatted: Font: Italic

Deleted: protein

Deleted: to

Formatted: Font: Italic

Formatted: Font: Italic

Deleted: )

Formatted: Font: Italic

Formatted: Font: Italic

Deleted: ,

Deleted: *Haemonchus*

Deleted: *C.*

Deleted: *briggsae*

Formatted: Font: Italic

Deleted: species

Deleted: ancylostomatidae

Deleted: as

352 the presence of eggs in female utero, the subset of DE genes with a one-to-one ortholog in *C. elegans* was  
353 considered to remove any gene known to be expressed in the oocyte, the germ line or the embryo (data  
354 retrieved using the wormbase.org “simple mine” online tool). Genes with unknown expression patterns in *C.*  
355 *elegans* were not considered. While this subset remains artificial in nature, it offers a gene population whose  
356 differential expression between males and females was deemed independent of the presence of eggs in female  
357 worms.

### 358 Spatio-temporal sampling of *C. nassatus* diversity using a pool-sequencing framework

359 The sampling scheme pursued two objectives driven by the understanding of the evolution of drug resistance  
360 in cyathostomin populations. First, spatio-temporal sampling was applied to establish the degree of  
361 connectivity among populations of Western Europe and North America, including isolates from western  
362 Ukraine (n = 1), Germany (Hannover region, n = 1), France (Normandy, n = 4; Nouzilly, n = 1) and American  
363 (Kentucky, n = 1). French samples consisted of the isolate used for genome assembly and four other populations  
364 were collected in Normandy (Calvados département, within a 30 km radius; note that latitude and longitude  
365 have been voluntarily modified to ensure anonymity of the sampled stud farms). In that case, two pyrantel-  
366 resistant isolates were geographically matched with pyrantel-susceptible isolates. Pyrantel-resistant worms  
367 were exposed to pyrantel embonate (Strongid<sup>®</sup>, 6.6 mg/kg, Zoetis, France) to first confirm their resistance  
368 potential 14 days after treatment, and finally recovered 24 h after ivermectin (Eqvalan pate, 200 µg/kg,  
369 Boehringer Ingelheim animal health, France) treatment. Pyrantel sensitivity (measured as a Faecal Egg Count  
370 Reduction coefficient) was estimated using the eggCounts package (Wang et al. 2018) for the Normandy  
371 isolates, while previously published data from France (Boisseau et al. 2023) and American isolates (Scare et al.  
372 2018) were used for the reference.

373 For every population, single male worms were considered and genotyped for the ITS-2 and COI barcodes  
374 (Courtot et al. 2023) to ascertain their identity. DNA was extracted using the same salting-out protocol as  
375 before, quantified using a Qubit apparatus, and pooled together with an equimolar contribution of each  
376 individual worm to the pool. The Ukrainian population consisted of 100 worms sampled after ivermectin  
377 treatment across Ukrainian operations and morphologically identified (Kuzmina 2012). Their DNA was  
378 extracted en-masse and used for pool-sequencing.

379 A museum sample collected in 1899 by Prof. Arthur Looss in Egypt, fixed in 70% ethanol, identified  
380 morphologically and preserved in the Swedish Museum of Natural History (Kuzmina and Holovachov 2023) was  
381 also included in the study to compare pre-anthelmintic diversity to that observed in contemporary samples. To  
382 deal with this old material, the previously described extraction protocol (Gamba et al. 2016) was adapted as  
383 follows. Briefly, worms were digested in a lysis buffer for 3 hours at 56 °C. Worm lysate was subsequently  
384 processed using the DNA clean-up kit (Macherey-Nagel) using the washing solution in a 4-to-1 excess to retain  
385 as much material as possible. Elution buffer was heated at 70 °C for DNA recovery in a final volume of 20 µL.

386 Due to the small size of the starting DNA material, the pool-seq library was constructed using the Accel NGS 2S  
387 Plus DNA Library Kit (Swift Biosciences, ref. SW21024) without any fragmentation step. Briefly, we end-repaired  
388 the fragments before indexed adapter ligation. We performed 9 cycles of PCR amplification on the indexed  
389 DNA. The size distribution of the resulting library was monitored using a Fragment Analyzer with the High  
390 Sensitivity NGS kit (Agilent Technologies, Santa Clara, CA, USA) and the library was quantified using the KAPA  
391 Library quantification kit (Roche, Basel, Switzerland).

392 The library was denatured with NaOH, neutralised with Tris-HCl, and diluted to 200 pM. Clustering and  
393 sequencing were performed on a NovaSeq 6000 (Illumina, San Diego, CA, USA) using the single read 100 nt  
394 protocol on 1 lane of a flow cell SP. Image analyses and base calling were performed using the Miniseq Control  
395 Software and the Real-Time Analysis component (Illumina). Demultiplexing was performed using Illumina's  
396 conversion software (bcl2fastq 2.20.0.422). The quality of the raw data was assessed using FastQC (v0.11.9)  
397 from the Babraham Institute and the Illumina software SAV (Sequencing Analysis Viewer). FastqScreen was  
398 used to identify potential contamination.

400

Deleted: were

Deleted: from

Deleted: a

Deleted: département

Deleted: Km

Deleted: pyrantel

Deleted: to first confirm their resistance potential

Deleted: hours

Deleted: treatment

Deleted: .

Deleted: were used for the reference

Deleted: .

Deleted: equi-molar

Deleted: . In that case, worms were identified morphologically

Formatted: Superscript

Deleted: were end-repaired

Deleted: a

418 **Pool-sequencing data processing and SNP calling**

419 After adapter trimming using cutadapt v.3.4, genomic data were mapped onto the reference using bwa-mem2  
420 v2.2, retaining properly mapped reads with quality phred score above 20 with samtools v1.9. Duplicate reads  
421 were identified and filtered using Picard v.2.20.7 (Anon 2019) and indel realignment was applied using GATK  
422 v3.8 (McKenna et al. 2010). The pre-processed data were subsequently treated with the Popoolation2 software  
423 to generate a sync file, considering a minimum quality phred score of 30 and removing regions falling within 5  
424 bp from an indel.

425 Genome-wide nucleotide diversity was estimated within 5 kbp windows, with a minimal read depth of 10 using  
426 npstats (Ferretti et al. 2013). The average nucleotide diversity estimates were used as an initial guess for SNP  
427 calling using snape-pooled v2.8 software (Raineri et al. 2012) applied on filtered mpileup files (-C 50 -q 20 -Q  
428 30 -d 400). The sites with 90% support were retained as high-quality SNPs, and the intersection between the  
429 snape-pooled SNPs and popoolation2 sites was further considered for analysis.

430 This approach was applied to the whole set of populations for the study of genome-wide diversity (n =  
431 23,384,719 autosomal SNPs supported by one read across pool; n = 514,068, after filtering for a depth of  
432 coverage between 20 and 400x, a minor allele frequency of 5%) or restricted to the set of six modern  
433 populations with pyrantel efficacy data (n = 36,129,276 autosomal SNPs and 2,807,924 SNPs on the X  
434 chromosome) for the association study.

435  
436 **Investigation of genome-wide diversity and pyrantel resistance architecture**

437 Nucleotide diversity and Tajima's D statistics were estimated for 100-Kbp sliding windows with npstats v2.8  
438 from the high-quality SNP set provided as a bed file. Investigation of genome-wide diversity was subsequently  
439 performed on the set of SNPs shared across old and modern populations after filtering for sites with minimum  
440 coverage below 15, maximum coverage above 400 and minor allele frequency below 5% with the poolfstat  
441 package v2.0.0 (Gautier et al. 2022). Private variants were selected from the set of unfiltered autosomal SNPs,  
442 isolating markers with a minimal depth of coverage of 10 in every pool but absent in all but the focal isolate.  
443 Reference allele frequencies were binned by 10% MAF for plotting. Population connectivity was investigated  
444 using a principal component analysis applied to folded allele frequencies using the pcadapt (Luu et al. 2017) R  
445 package v4.3.3 and the set of filtered SNPs (n = 1,346,424). Genetic differentiation ( $F_{ST}$ ) and admixture statistics  
446 ( $f_3$  and  $f_4$ ) were estimated using the ANOVA method of the poolfstat v2.0.0 (Gautier et al. 2022).

447 To isolate genomic regions associated with pyrantel susceptibility, we regressed allele frequencies upon scaled  
448 population pyrantel efficacy while accounting for population genomic relatedness using the Baypass software  
449 v2.2 (Gautier 2015). The modern population SNP set was filtered using the poolfstat (Gautier et al. 2022) R  
450 package to retain sites with a pool coverage between 10 and 400, a minimal MAF of 5% and 4 reads to support  
451 an allele leaving 8,365,939 and 1,049,048 SNPs on the autosomes and X chromosome respectively. The analysis  
452 was run on 15 pseudo-replicates of 557,727 to 557,732 autosomal SNPs (69,936 to 69,936 for the X  
453 chromosome) and averaged from six independent runs (-npilot 15 -pilotlength 500 -burnin 2500). For the X  
454 chromosome, the analysis was run on the five isolates composed of males. Any variant with a Bayes factor  
455 above 35 was deemed decisive, while significance was decided upon a Bayes factor of 20. QTL regions were  
456 defined as the extreme edges of contiguous 1-Mbp windows with more than 10 decisive SNPs. Within these  
457 windows, three strands of evidence were considered to be called candidate genes. First, the known candidate  
458 genes for pyrantel resistance (*unc-29*, *unc-38*, and *unc-63*) were inspected for the presence of significant SNPs  
459 within their locus or in their vicinity. A second prior-informed approach consisted in inspecting homologs of *C.*  
460 *elegans* genes affected by aldicarb (<https://wormbase.org/resources/molecule/WBMol:00003650#032--10-3>,  
461 last accessed May 24<sup>th</sup> 2023) or levamisole  
462 (<https://wormbase.org/resources/molecule/WBMol:00004019#032--10-3>, last accessed May 24<sup>th</sup> 2023), two  
463 molecules affecting the effect of acetylcholine at the neuro-muscular junctions. Third, enrichment analysis was  
464 run using the *C. elegans* homologs with one-to-one or many-to-one orthology (e.g. four copies of *unc-29*) and  
465 the wormbase online enrichment tool (Lee et al. 2018). Fourth, the decisive SNPs within gene loci showing a  
466 correlation between allele frequency and the measured FECRT above 90% were regarded as strong candidates  
467 for field use, as their association would not be affected by population structure.

Deleted: were

Deleted: x

Deleted: high

Deleted: "anova"

Deleted: call

473

474 ***C. elegans* pyrantel-resistant line selection and RNAseq analysis**

475 To generate pyrantel-resistant lines of *C. elegans*, a large population of wild-type N2 worms was produced from  
476 four L4 on 10 different NGM (Nematode Growth Medium) plates. All worms from this founder population were  
477 collected with M9 medium and pooled, before being transferred to new plates containing 20 µM pyrantel (IC<sub>20</sub>  
478 allowing 80% of worms reaching adulthood) or not, with 6 different replicates for each condition. Once the  
479 worms survived and reproduced (generally at least two generations per concentration) at a given  
480 concentration, they were transferred to a plate with a higher pyrantel concentration with 20-µM increase until  
481 survival at 100 µM was reached. This resistance level was reached after 12 generations. Total RNA extractions  
482 were performed using Trizol reagent (Invitrogen, Carlsbad, CA, USA) and total RNA was isolated according to  
483 the manufacturer's recommendations. Briefly, worms from each condition were recovered with M9 and  
484 washed with M9, 3 times, before being resuspended in 750µL Trizol. They were then ground with the Precellys  
485 24 Homogenizer (Bertin, France) using 10-15 glass beads (0.5 mm) and the following program: 6400 rpm, 10 s  
486 two times, twice for a total time of 40 s. After grinding, 250µL of Trizol were added to reach a final volume of  
487 1 mL. A DNase treatment step was performed using rDNase from the NucleoSpin RNA XS kit (Macherey-Nagel,  
488 Germany) and the RNA concentrations were measured using a nanodrop spectrophotometer.  
489 RNA library preparations, and sequencing reactions for both the projects were conducted at GENEWIZ  
490 Germany GmbH (Leipzig, Germany) as follows. RNA samples were quantified using Qubit 4.0 Fluorometer (Life  
491 Technologies, Carlsbad, CA, USA), and RNA integrity was checked with RNA Kit on Agilent 5600 Fragment  
492 Analyzer (Agilent Technologies, Palo Alto, CA, USA).

493 The strand-specific RNA sequencing library was prepared by using NEBNext Ultra II Directional RNA Library Prep  
494 Kit for Illumina following the manufacturer's instructions (NEB, Ipswich, MA, USA). Briefly, the enriched RNAs  
495 were fragmented for 8 minutes at 94°C. First-strand and second-strand cDNA were subsequently synthesised.  
496 The second strand of cDNA was marked by incorporating dUTP during the synthesis. cDNA fragments were  
497 adenylated at 3'ends, and indexed adapters were ligated to cDNA fragments. Limited cycle PCR was used for  
498 library enrichment. The dUTP incorporated into the cDNA of the second strand enabled its specific degradation  
499 to maintain strand specificity. Sequencing libraries were validated using DNA Kit on the Agilent 5600 Fragment  
500 Analyzer (Agilent Technologies, Palo Alto, CA, USA), and quantified by using Qubit 4.0 Fluorometer (Invitrogen,  
501 Carlsbad, CA).

502 The sequencing libraries were multiplexed and clustered onto a flow-cell on the Illumina NovaSeq instrument  
503 according to the manufacturer's instructions. The samples were sequenced using a 2x150bp Paired End (PE)  
504 configuration. Image analysis and base calling were conducted by the NovaSeq Control Software (NCS). Raw  
505 sequence data (.bcl files) generated from Illumina NovaSeq was converted into fastq files and de-multiplexed  
506 using Illumina bcl2fastq 2.20 software. One mis-match was allowed for index sequence identification.

507 Data were analysed using a similar framework as that applied to the sex-specific differential transcriptomic  
508 analysis using pseudo-mapping and performing differential analysis with the DESeq2 package (Love et al. 2014).

509

Formatted: Font: Italic

Deleted: First

Deleted: second

Deleted: x

513  
514  
515  
516  
517  
518  
519  
520  
521  
522  
523  
524  
525  
526  
527  
528  
529  
530  
531  
532  
533  
534  
535  
536  
537  
538  
539  
540  
541  
542  
543  
544  
545  
546  
547  
548  
549  
550  
551  
552  
553  
554  
555  
556  
557  
558  
559  
560  
561  
562

## Results

### The chromosome-shape assembly of *C. nassatus* defines an XO/XX karyotype

A reference genome was built from a single *C. nassatus* worm using PacBio long reads to build contigs which were scaffolded with Hi-C reads (Fig. 1a, S1, Table S1) generated from a pool of 70 worms from the same isolate. This was part of a larger initiative that also produced long-read data for five other species including *Coronocylcus labiatus*, *Cyathostomum catinatum*, *Cylicostephanus goldi*, *Cylicostephanus longibursatus* and *Cylicocylcus insigne* (The cyathostomin genomics consortium 2023).

The first round of assembly using HiFi reads yielded a 666.9 Mbp sequence fragmented in 2,232 contigs after haplotype purging. Hi-C sequencing yielded 525 M read pairs, 55.41% of which being alignable to the assembly (Fig. S1). Among these, 135,180,104 chromatin contacts were identified with an equal representation of inter- (n = 69,144,270) and intra-chromosomal (n = 66,035,834) levels and 36% of these contacts being found at 20 Kbp. Following Hi-C data curation, a chromosome-scale assembly of 514.7 Mbp was built (scaffold N50 = 91,661,033 bp, scaffold L50 = 3; contig N50 = 674,848 bp; Table 1, Fig. 1a, Fig. S1) with high degree of completeness as supported by the 85.8% complete BUSCOs found that slightly outperformed the *H. contortus* genome statistics of 82.7%. The difference between the two genome assemblies mostly owed to higher missing BUSCOs in the *H. contortus* assembly (9.6%, n = 300) relative to *C. nassatus* (6.4%, n = 203).

After RNA-seq informed gene model prediction, the genome was 94.1% gene complete (n = 2,841 single-copy and 188 duplicated BUSCOs) and 4.4% missing identifiers (n = 136). The annotation comprised 22,718 coding genes, with an average of 4,010.4 genes (ranging between 4,152 and 3,831 genes) sitting on the five larger chromosomes. Gene length (1,286 bp on average, range between 153 and 79,776 bp) was well correlated with the number of exons (Pearson's  $r = 0.76$ ,  $P < 10^{-4}$ ) that could reach as high as 252 exons (CNASG00031410, chromosome I). Total interspersed repeats covered 50.07% of the assembly sequence (Fig. 1, Table S2, Fig. S2). Most of them (n = 656,357) were unclassified or otherwise falling in the LINEs (5.06% of sequence length), LTRs (1.89% of sequence length), or the Tc1/Mariner DNA families (n = 2,998 elements) (Fig. S2). This pattern matches the previous description of the trichostrongylid *H. contortus* genome although fewer elements were unclassified in that case (n = 292,099, Doyle et al. 2020).

Six major linkage groups defining nuclear chromosomes with evidence of telomeric repeats accounted for 97% of the assembly size. A 13,878 bp mitochondrial genome was resolved from single HiFi reads. Nuclear chromosome lengths ranged between 107.7 and 83.5 Mbp for five of them and a smaller sequence of 34.4 Mbp (scaffold 6). Using several strands of evidence, this chromosome likely defines the X chromosome whose dosage is associated with sex in other clade V nematode species. First, a  $27.8x \pm 0.9$  drop in depth of coverage was observed for that chromosome in re-sequenced male populations ( $t_1 = -30.85$ ,  $P < 10^{-4}$ , Fig. 1b), and its coverage was halved in pools of males relative to the pools containing males and females ( $\beta_{\text{Males \& females}} \times X = 34.4 \pm 1.8$ ,  $t_1 = 19.04$ ,  $P < 10^{-4}$ , Fig. 1b). Second, windowed estimates of nucleotide diversity in male worms were also significantly reduced on this chromosome relative to that observed on the rest of their genome ( $\pi_{\text{chr1}} = 0.008687 \pm 3.070 \times 10^{-6}$ ,  $\pi_{\text{chr6}} = 0.007662 \pm 1.154 \times 10^{-5}$ ,  $t_{81732} = 98.9$ ,  $P < 10^{-4}$ , Fig. 1c). Third, this scaffold showed marked synteny with *H. contortus* X chromosome (42.5% of the 762 alignments involving scaffold 6; Fig. S3). Last, the genes found on this chromosome were more often up-regulated in female worms relative to their male counterparts (54.4% of DE genes), whereas the opposite was true on the other five chromosomes (35 to 49% of the DE genes, Fig. 1a). This likely X chromosome showed a denser gene content (55.2 genes/Mbp vs. 43.08 genes/Mbp for the five larger chromosomes) and longer gene length (282.27 bp  $\pm$  37.68 more than on the other five chromosomes,  $t = 7.49$ ,  $P < 10^{-4}$ ). Repeat elements also appeared relatively contained to chromosome arms (50% of repeat elements within the first and last 10 Mbp).

The estimated species tree (from 2,387 orthogroups shared across the selected species; n = 30,491 orthogroups in total), supported the intermediate phylogenetic position of *C. nassatus* between Ancylostomatoidae and Trichostrongyloidae as previously found for *C. goldi* (International Helminth Genomes 2019) (Fig. 1d).

In the lack of karyotyping data for any cyathostomin species, this fully resolved assembly defines a six-chromosome genome and a XX (female)/ XO (males) sex determination as seen in the trichostrongylid *H. contortus* or free-living caenorhabditids.

Formatted: Font: Italic

Deleted: long

Deleted: t

Deleted: ,884 Kbp

Formatted: Font: Italic

Formatted: Font: Italic

Formatted: Font: Italic

Deleted: range

Formatted: Font: Italic

Formatted: Font: Italic

Deleted:

Formatted: Font: Italic

Deleted:

Formatted: Font: Italic

Formatted: Font: Italic

Formatted: Font: Italic

Formatted: Font: Italic

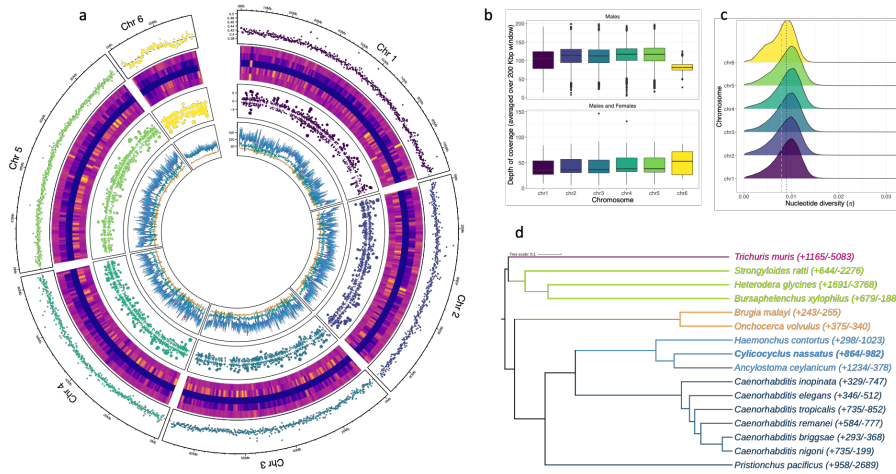


**Figure 1. Structure of the *Cylicocyclus nassatus* genome**

a. The circos plot consists of six tracks for each chromosome assembled, with their averaged GC-content presented on the outer ring. The heatmap corresponds to the content in identified repetitive regions, with the overall content, DNA, LINE, LTR, and other families presented towards the center of the plot. The third layer represents the differentially expressed genes (represented as log fold change; dot size is proportional to this value) found between males and females taken as the reference level (positive values indicate over-expression in males). The innermost track shows the average depth of coverage for nine re-sequenced populations. b. Distribution of windowed depth of coverage across the six major scaffolds in male-only or female and male populations (bottom). c. Nucleotide diversity distribution for each chromosome. The orange and blue lines stand for the mean  $\pi$  value of chromosome 6 or that of other chromosomes, respectively. d. Phylogenetic tree (estimated from 2,387 protein sequences) showing gene family evolution (expanded or contracted; numbers in brackets) across parasitic nematode species of interest (coloured by clades).

**Allele frequencies of known anthelmintic targets have changed over the last century.**

The genome-wide diversity of *C. nassatus* populations was investigated from nine populations sampled across five countries (Fig 2a), including an older population sampled from Egypt at the end of the 19th century. The windowed depth of coverage was 38.6x on average (Fig 2b) but lower in the older sample and in the Hi-C derived dataset from the reference population (18x in both cases). Despite DNA fragmentation of the old sample, the data yielded an even representation of the whole genome (Fig. S6) and did not show evidence of strong degradation (Fig. S7).

*Cylicocyclus nassatus* genetic diversity was high as illustrated by the 23,384,719 autosomal Single Nucleotide Polymorphisms identified or their average genome-wide nucleotide diversity estimates ranging from  $6.06 \times 10^{-3}$  in the reference population to  $9.07 \times 10^{-3}$  in the old isolate (Fig. 2b, table S4). These estimates would be compatible with an average effective population size of 766,102 individuals.

**Deleted:  $\pi$**

**Deleted: Gene family evolution ¶**

The estimated species tree (from 2,387 orthogroups shared across the selected species;  $n = 30,491$  orthogroups in total), supported the intermediate phylogenetic position of *C. nassatus* between Ancylostomatoidea and Trichostrongyloidea as previously found for *C. goldi* (International Helminth Genomes 2019) (Fig. 1d). ¶ Using the 10,221 hierarchical orthogroups (HOGs) present at the root of this phylogeny, the *C. nassatus* genome presented 864 and 982 expansions and contraction events respectively, following the divergence with *Ancylostoma ceylanicum* (Fig 1d, Table S3). Out of these, 134 corresponded to rapid evolution ( $n = 36$  contractions,  $P < 1\%$ , Fig. 1d, S4). The most significant gene family evolution was the rapid expansion (+36 genes,  $P = 2.43e-33$ , table S3, Fig. S4) of genes coding for voltage gated potassium channel tetramerization determinants that facilitate the assembly of the alpha-subunits to form a functional channel (Pfaffinger et al. 2000). These homologs of F18A11.5 in *C. elegans*, were almost entirely confined to a 798-kb window of chromosome I ( $n = 19$  out of the 27 genes harboured on that chromosome) laying 13.394 Kbp up-stream of two unc93-like genes found in *A. ceylanicum* (CNASG00033450, homolog to Acey\_s0067.g23, 70% identical, e-value = 6.09e-233) or *Necator americanus* (CNASG00033430, homolog to NAME\_11930, 66% identical, e-value = 2.32e-168). Other significant expansions included homologs of C-type lectins (+48 genes,  $P = 1.17e-29$ ; table S3) and pogo transposable elements with KRAB domain (POGK; +24 genes,  $P = 4.92e-25$ ). This rapid increase in DNA transposons may entertain a causal relationship with the increase in *C. nassatus* genome size relative to that of *A. ceylanicum* (Schwarz et al. 2015) and *H. contortus* (Doyle et al. 2020). ¶ Of note, another HOG under rapid expansion (HOG0000865, +10 genes,  $P = 7.4246e-06$ , table S3) contained five genes harbouring Phlebovirus glycoprotein G2 fusion domain (PF07245), a feature of endogenous viral elements recently described in the *A. ceylanicum* genome (Merchant et al. 2022). Among the 27 genes assigned to this HOG, six had EggNOGg homology to *A. ceylanicum* EVEs (Y032\_0203g1846 and Y032\_0070g451 proteins) with protein similarity ranging from 39.7 to 58.1% and a coverage of 91.4%. Active transcription was found for nine members of this HOG (Fig. S5), including four homologs of the *A. ceylanicum* EVEs (CNASG00027320, CNASG00122160, CNASG00189380, CNASG00213220) whereby the ... [1]

**Formatted: Font: Italic**

**Deleted: The last century affected allele frequencies over known anthelmintic drug targets**

Deleted: XIX

Deleted: x

Deleted: x

Deleted: x

Deleted: x

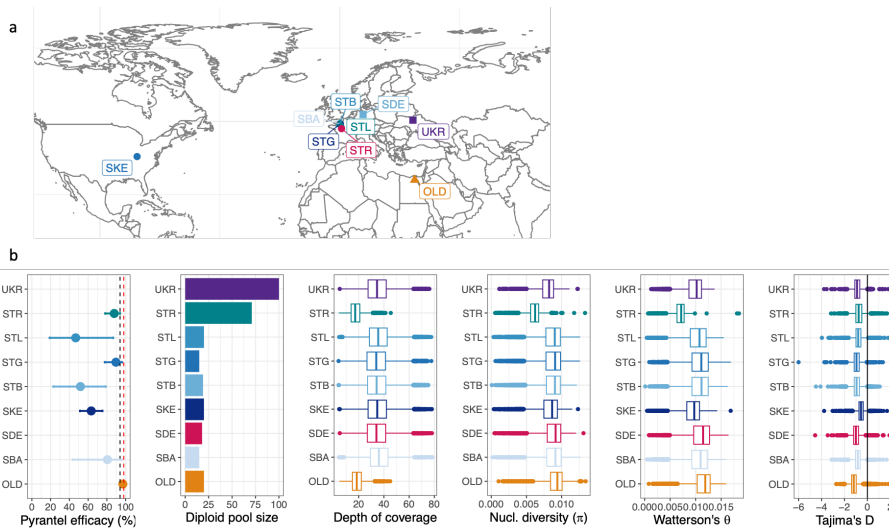


**Figure 2. Genome-wide diversity in modern and old *Cylicocyclus nassatus* isolates**  
 a. Isolate repartition. b. Isolate sensitivity to pyrantel (black and red dashed lines correspond to original and targeted efficacies). Pool composition, windowed depth of coverage, and genome-wide diversity coefficients distribution are represented for every isolate (OLD: 19th-century Egyptian isolate; SBA, STB, STG, and STL: four stud farms from Normandy, France; SDE: Hanover region, Germany; SKE: Kentucky, USA; STR: reference isolate, Nouzilly, France; UKR: Ukraine).

The old Egyptian worms had both the highest nucleotide diversity estimates (0.087% difference with modern isolates,  $t = 37.19$ ,  $P < 10^{-4}$ ) and the highest count of private variants, which would be compatible with a global loss of diversity in *C. nassatus* populations in the sampled isolates over the last century or higher diversity within African worms. Investigation of that latter hypothesis would require contemporary Egyptian worms that were not available for this study. The most extreme variance in allele frequencies between the 19th and 21st century isolates ( $n = 1,267$  outlier windows of 100 SNPs; Fig. S8) occurred on chromosomes 2 ( $n = 748$ , Fig. S9) and 5 ( $n = 290$ , Fig. S10). Consistent outlier signals ( $n = 7$  out of 8 comparison) were found over five genes coding for homologs of a D-aspartate oxidase (*ddo-1* and *ddo-2* in *C. elegans*) or lipase-domain containing genes (CNASG00085640, CNASG00085630). On chromosome 2, the signals were enriched over QTL regions associated with pyrantel resistance (see paragraph 5, Fig. S9) and a single outlier window (between the old and Kentucky isolate) encompassed the  $\beta$ -tubulin isotype-1 locus (CNASG00077300) known to confer resistance to benzimidazoles (Kwa et al. 1993) (Fig. S9). No signal was found over the  $\beta$ -tubulin isotype-2 coding gene on chromosome 5 (Fig. S10). Along with these known drug-resistance candidate genes, outlier differentiation occurred over homologs of nAChR subunit coding genes sitting on chromosome 2, namely *unc-63* and three homologs of *unc-29* (see paragraph 5, Fig. S9).

**The connectivity of *C. nassatus* populations is compatible with ancient and pervasive admixture from Eastern Europe**

Most SNPs were private to each isolate (between 51,580 and 375,369 SNPs; Fig.3a), with only 1,346,424 common SNPs matching the filtering criteria. Private variants segregated (98% of 1,801,440 SNPs) at low frequencies (<30%), especially in the Ukrainian isolate suggestive of important gene flow in this region (Fig. 3a). On the contrary, the American isolate displayed 113 sites with frequency of 60% and higher (Fig. 3a), reflecting accumulation of private variants permitted by their lower genetic connectivity to Europe, owing to both geographical distance and the isolation of their hosts since 1979.

Deleted: 19XIX<sup>th</sup> century

Deleted: indicate

Deleted: XIX

Deleted: XXI

Formatted: Font: Italic

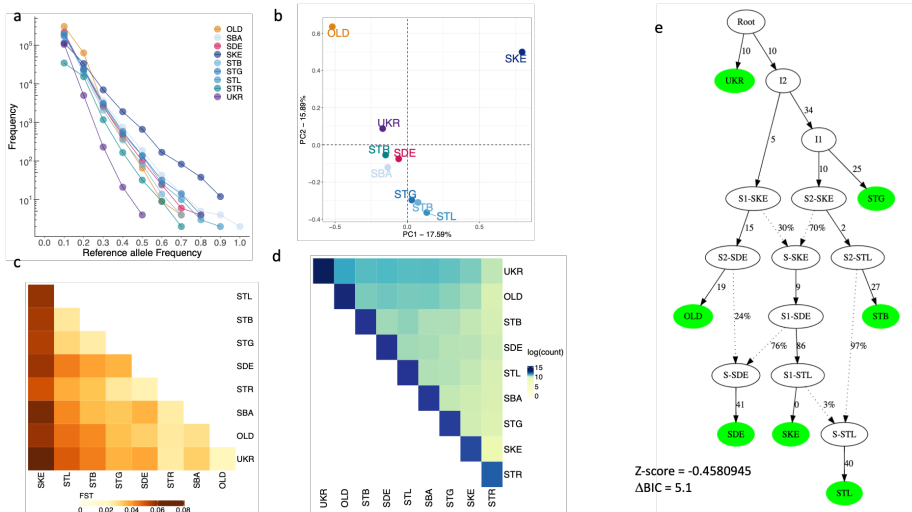
Formatted: Font: Italic

Formatted: Font: Italic

Deleted: drug

704  
705  
706  
707  
708  
709  
710  
711  
712  
713  
714  
715  
716  
717  
718  
719  
720  
721  
722  
723  
724  
725  
726  
727  
728  
729  
730  
731  
732  
733  
734

740 The connectivity inferred from private variants was mirrored in the PCA on folded SFS, whereby the east-west  
 741 gradient broadly defined the first component with the old Egyptian and contemporary American isolates  
 742 positioned at each end (Fig. 3b, S11). The second PCA axis was driven by the disconnection between these two  
 743 samples from the modern European cluster (Fig. 3b) and could reflect a temporal gradient, either owing to old  
 744 variants present in 1899 in the Egyptian worms, or to the putative sampling of older ancestry (native or  
 745 imported) in American worms. The close relationship entertained by modern European worms was evident on  
 746 other components and would also suggest admixture between these isolates (Fig. 3b, S11). Similarly, the  
 747 genetic differentiation was also driven by the east-west gradient in a set of otherwise lowly differentiated  
 748 isolates (global  $F_{ST} = 0.041$ , 95% c.i. = 0.04 - 0.042; Fig. 3b). Last, while the negative Tajima's  $D$  found in every  
 749 population would also suggest on-going admixture (Table S4), higher values were observed for the populations  
 750 from closed herds (SKE, Tajima's  $D = -0.419 \pm 0.69$  for the Kentucky isolate, and  $-0.482 \pm 0.86$  for the reference  
 751 STR isolate; Fig 3b). Despite these strands of evidence in favour of pervasive admixture,  $f_3$  coefficients - that  
 752 measures the degree of resemblance between one population and two other source populations - were non-  
 753 significant ( $|Z\text{-score}| > 12$ ). This is compatible with either too little or too high admixture between populations,  
 754 or genetic drift in the focal isolate erasing the signal since admixture.  
 755



756  
 757 **Figure 3. Pervasive gene flow defines old and modern *Cylicocyclus nassatus* isolates**

758 a. The number of private SNPs for a given isolate with allele frequency below or equal to the allele frequency displayed on the x-  
 759 axis. b. Projection of the isolates on the first two components of a PCA on allele frequencies (n = 1,223,750 SNPs). c. Heatmap of  
 760 pairwise counts of SNPs observed only twice in the set of common SNPs. d. Heatmap of genetic differentiation coefficient  
 761 estimated from 1,223,750 SNPs spanning chromosomes 1 to 5 (the darker, the most differentiated). e. Admixture graph with best  
 762 statistical support connecting the seven isolates from every sampled continent, with branch length given in drift units. Isolate  
 763 abbreviations match figure 2 caption.  
 764

765 In line with the latter hypothesis, we found significant evidence of shared ancestry between four French  
 766 populations at lower allele frequencies (MAF < 20%, n = 254,604 SNPs). In each case, the  $f_3$  with highest support  
 767 consistently involved the Ukrainian isolate as a source proxy, in combination with other isolates of Normandy  
 768 or German origins (Fig. S12a). This would be compatible with a contribution from an Eastern-related population  
 769 in relatively recent times that is absent or has been lost at higher frequencies. Of note, Ukraine retained most  
 770 of the older variation as illustrated by the low genetic differentiation they entertained ( $F_{ST} = 0.022$ , Fig. 3c) and

Deleted: to

772 the highest share of old variants (Fig. 3d, n = 70,283 SNPs). This Eastern contribution had also the best support  
773 for admixture events detected in the old worms when considering high frequency variants (MAF >70% in every  
774 population, n = 351,262; Fig. S12b). These strands of evidence would hence suggest that the Eastern European  
775 contribution to *C. nassatus* ancestry is pervasive and precedes the 19<sup>th</sup> century. Consistent with this pattern,  
776 the most likely admixture graph (Fig. 3e, S13) was compatible with a founder population closely related to the  
777 Ukrainian worm populations and from which all other isolates derived. In that scenario, successive admixture  
778 events between past populations sharing ancestry with the German and Kentucky isolates would have defined  
779 the European, American, and Egyptian isolates (Fig. 3e).

#### 781 **Transcriptomic differences across sexes upon pyrantel exposure**

782 Cyathostomin (reference isolate, STR) collection upon pyrantel treatment of their host indicated a disbalanced  
783 sex-ratio whereby three times more females than males were collected over the considered 9-hour window  
784 ( $\beta_{sex} = 1.08 \pm 0.28$ ,  $t_{66} = 3.917$ ,  $P = 2 \times 10^{-4}$ ; Fig. 4a, S14). This 20% male-to-female ratio was lower than previous  
785 reports ranging from 0.4 to 0.6 (Silva et al. 1999; Anjos and Rodrigues, 2006; Sallé et al, 2018). Transcriptomic  
786 differences between males and females (three pools of four to five males and three pools of three to four  
787 females) collected after pyrantel treatment were quantified. Inspection of gene count distribution revealed a  
788 bimodal distribution in females (centred at a median count cut-off of 608, Fig. 4b), applying over every  
789 chromosome (Fig. S15) and reflecting the transcriptomic contrast between the female body and their  
790 reproductive tract and the developing eggs it harbours (Fig. S15, tables S5 and S6). This was also mirrored in  
791 the 2,600 genes up-regulated in females (out of 5,860 differentially expressed between sexes, table S7) that  
792 defined significant enrichment for 120 biological processes, with an overwhelming contribution of nucleic acid  
793 metabolism, or chromatin organisation and segregation (Table S8) compatible with egg division and  
794 production. In this respect, 138 genes were related to embryo development ending in birth or egg hatching  
795 (GO:0009792,  $P = 7.5 \times 10^{-4}$ , Fig. 4c, Table S8). In sharp contrast, male worms expressed higher levels of  
796 transcripts related to ion homeostasis and pH regulation (n = 7 terms, Table S8), muscle contraction and  
797 metabolism (n = 4 terms, Table S8), neuronal system (n = 2 terms, Table S8), or pyrimidine-containing  
798 compound catabolic process (GO:0072529,  $P = 3.98 \times 10^{-2}$ ).

799 To delineate somatic transcriptional differences between males and females not owing to the presence of eggs  
800 in utero, we selected *C. nassatus* DE genes with a one-to-one ortholog in *C. elegans* that were not known to be  
801 expressed in any of the oocyte, germ line, or embryonic stage of that model species. This process retained 148  
802 genes up-regulated in males whose ontology enrichment highlighted neuropeptide signal pathway  
803 (GO:0007218,  $P = 8.9e-05$ ), including orthologs of genes coding for FMRF like peptide (*flp-1*, -5, -17 and -21;  
804 Fig. 4d, Table S9). These genes were also associated with an over-representation of locomotion-associated  
805 phenotypes or acetylcholinesterase inhibitor response variants in *C. elegans* (Table S10, Fig. 4d). These data  
806 highlight the molecular substrates of sex differences in worms exposed to pyrantel.

Deleted: eastern

Deleted: XIX

Deleted: x

Deleted:

Deleted:

Deleted:

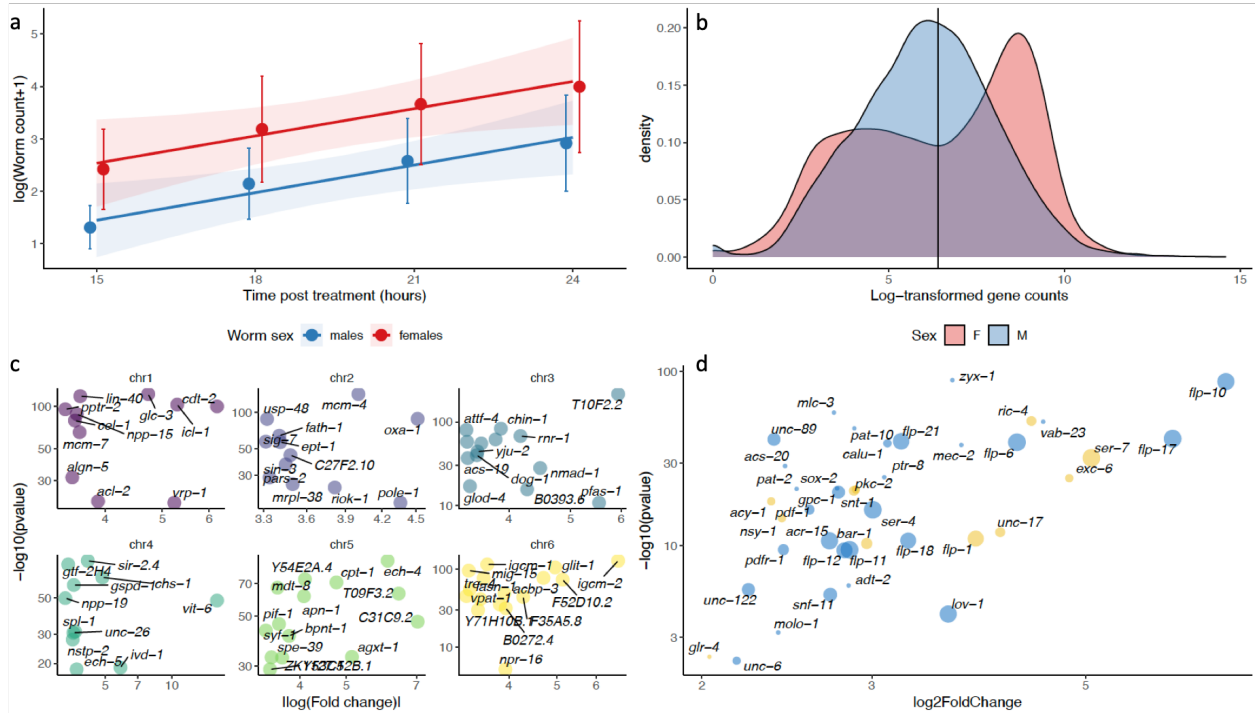
Deleted: To further understand this difference in *C. nassatus*, t

Deleted: This difference between sexes may either result from the differential nature of the transcripts between males and females as a consequence of the presence of developing eggs in female *utero*, or it may represent the basis of a sex-specific response to pyrantel treatment. To further distinguish between these two possibilities,

Deleted:

Deleted: ). that may point at candidates underpinning the differential sensitivity to pyrantel between sexes (Fig. 4d). ¶

Deleted: support sex-dependent sensitivity to pyrantel and define putative molecular substrates of worm plasticity to this drug.



828  
829  
830  
831  
832  
833  
834  
835  
836

**Figure 4. Differential expression between pyrantel-exposed males and females informs on differential response between the two sexes**  
**a.** Mean male and female cyathostomin (reference isolate, Nouzilly, France) counts (52.6% *C. nassatus* as inferred from larval metabarcoding (Boisseau et al. 2023)) collected between 15 and 24 hours after pyrantel treatment are represented along with the respective regression lines and confidence intervals. **b.** The distribution of the median log-transformed gene counts is represented for each sex, showing a bimodal distribution occurring in female *C. nassatus*. **c.** Female up-regulated genes are dominated by genes involved in embryo development. The absolute fold-change (relative to males) of the expression of the genes defining this GO term enrichment is plotted against their adjusted P-values. Panels match chromosomes and genes are annotated with their *C. elegans* orthologs when available. **d.** Genes up-regulated in males are enriched in locomotion-associated phenotypes in *C. elegans*. The size of each dot corresponds to the number of phenotype enrichments found in *C. elegans* and yellow dots indicate association with acetylcholinesterase inhibitor response variants.

Deleted: se

838

839 **A handful of Quantitative Trait Loci (QTL) underpin pyrantel resistance**

840 Transcriptomic data identified a plastic component of the response to pyrantel *in vivo* while the genes on which  
841 pyrantel selection acts upon may differ. To define the genetic landscape of pyrantel resistance, a genome-wide  
842 association analysis between SNP allele frequency and pyrantel resistance was run on six populations from  
843 France and Kentucky, USA (Fig. 5, S16, Table S11).

844

845 **Table 1. Quantitative Trait Loci (QTL) associated with pyrantel sensitivity with proposed candidate genes**

Chr.	QTL boundaries (bp)	Number of SNPs (total on chr.)	Candidate genes
1	87424141 – 88111850	14 (15)	<i>dkf-2*</i> , <i>erg-28*</i>
2	46547030 – 53471131	150 (167)	<i>ddo-3**</i> , <i>dys-1**</i> , <i>unc-29.4#</i> , <i>unc-29.1*#</i> , <i>unc-29.2*#</i> , <i>unc-29.3*#</i> , <i>gsnl-1**</i> , <i>rla-0**</i> , <i>yop-1**</i>
2	81892469 – 82887338	8 (167)	<i>chaf-1#</i> , <i>endu-1**</i> , <i>fer-1*</i> , <i>nduf-7**</i> , <i>rpl-24.1**</i>
4	21218710 – 21548186	27 (31)	<i>pqp-9</i>

846

847 Bold names were covered by at least one decisive Single Nucleotide Polymorphism (SNP), others had one significant SNP and  
848 were at most 20 Kbp away from a decisive SNP; #: affected by aldicarb in *C. elegans*; \*\*: enriched in the anal depressor muscle;  
849 #: physical interactants in *C. elegans*

850

851 This analysis found 222 SNPs with decisive association (Fig. 5, S16,17) on the five autosomes (43.7% and 83.3%  
852 falling within or 5-Kbp away from a gene locus) while 43 SNPs on chromosome X reached the significant level  
853 (BF > 20 dB; 48.8% falling within gene loci).

854

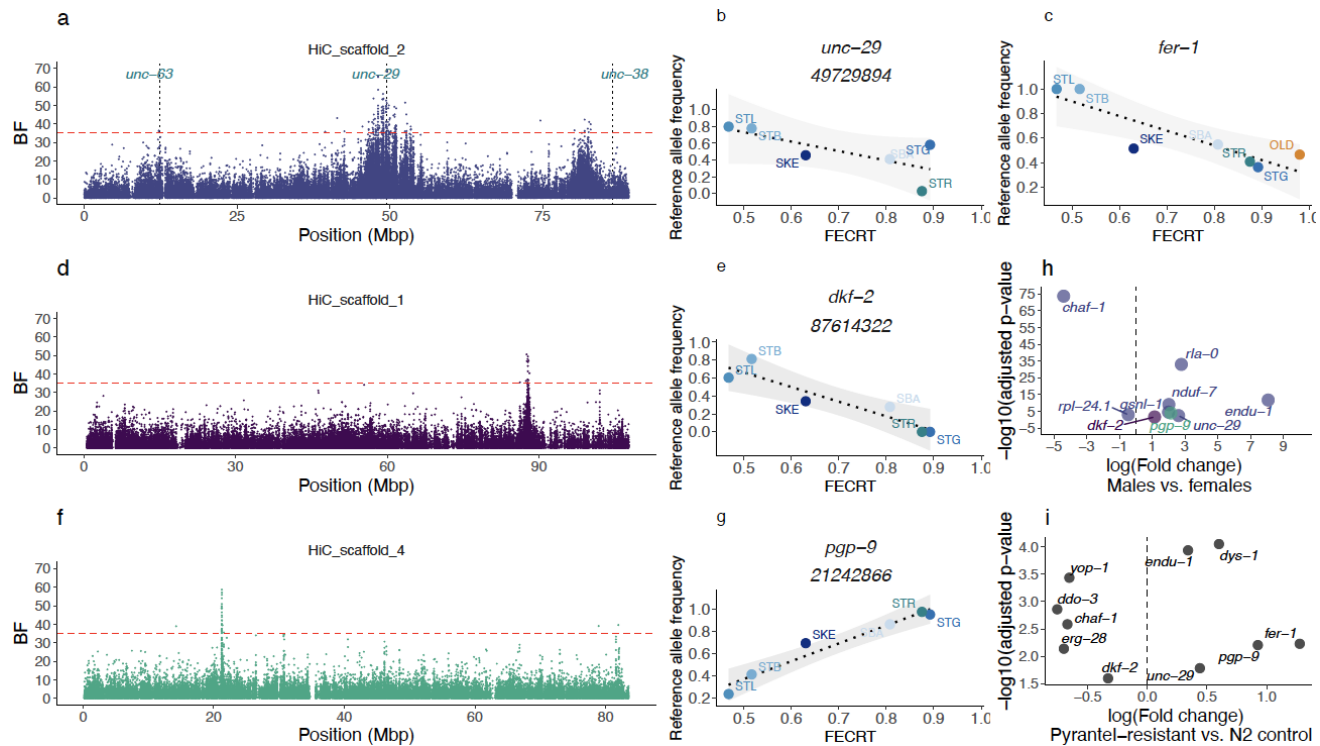


Fig. 5. Four Quantitative Trait Loci (QTL) regions define variation in pyrantel resistance

Left panels (a, d, f) represent the statistical support of the association (measured as a Bayes Factor, BF) between SNP allele frequency with pyrantel resistance on three chromosomes of interest (the red dashed line stands for the significance cut-off). The analysis was focused on contemporary isolates with known pyrantel sensitivity, i.e. four isolates from Normandy, France (two drug-resistant: STB and STL, and two drug-susceptible: SBA and STG), the reference drug-susceptible isolate (STR) and the drug-resistant isolate from Kentucky, USA (SKE). For each chromosome, the association between the raw allele frequency of the most likely candidate gene is plotted against the pyrantel sensitivity for every considered isolate (panels b & c for chromosome 2, e & g for chromosomes 1 and 4 respectively). (h) Differential gene expression profile (between male and female worms exposed to pyrantel) for the candidate genes laying within identified QTL regions (colours match the respective chromosomes as in panels a, d, f). i. Significance and expression fold change for the genes differentially expressed between control and pyrantel-selected *Caenorhabditis elegans* lines.

Deleted: The three l

Deleted: and

Deleted: for decisive associations

Deleted: after correction for population structure

Deleted: efficacy

Deleted: against each is given For each chromosome, allele frequency of the candidate genes is plotted against  $\eta$  Right panels fFor each chromosome and QTL region (right panels b, c, e, g), the raw allele (major reference allele) frequency of the likely causative SNP is plotted against each isolate pyrantel efficacy (FECRT: Faecal Egg Count Reduction Test; colours match those of Fig. 3a)

Deleted: .

Deleted:

878 The autosomal associations were enriched within four major QTL regions located on three autosomes (Tables  
879 1, S11) while chromosome 5 harboured another region with lower statistical support (Fig. S16, Table S11).  
880 Chromosome 2 - where homologs of three known candidates for pyrantel resistance (*unc-63*, *unc-29*, and *unc-*  
881 *38*) were found (Fig. 5a) - harboured 75% of the decisive SNPs that were enriched within a broad 6-Mbp region  
882 (46.5 to 53.5 Mbp, Fig. 5a) or a narrower peak centred at 82 Mbp (Table 1, Fig. 5a). These QTL regions also  
883 exhibited strong distortion of their allele frequencies between modern pyrantel-resistant isolates (and one  
884 pyrantel susceptible isolate) and 19th-century old worms (Fig. S8). On the 5' end of this chromosome, two  
885 significant associations were found over a homolog of *T15B7.1*, while the *unc-63* homolog was 104.372 Kbp  
886 downstream to these positions. However, none of the 154 SNPs found within the *unc-63* locus defined a robust  
887 association with pyrantel resistance (average BF = -6.032, max. = 13) and a single SNP 2,038 bp upstream  
888 (12,3030,713 bp) reached the significance level (20.6 dB). The same pattern applied over the *unc-38* locus (303  
889 SNP, average BF = -6, max = 11.67 dB) that was 3.5 Mbp downstream from the closest associated SNP  
890 (82,887,338 bp, dB = 37.0). On the contrary, the broader QTL region harboured four homologs of the *unc-29*  
891 gene (Fig. 5a), one of which (*CNASG00064360*) contains a single decisive SNP (Fig. 5b) and two others reaching  
892 significant association levels (five SNPs within *CNASG00064260* and one SNP over *CNASG00064350*). The genes  
893 (n = 1,636) found in this QTL region were associated with significant enrichment for locomotion (GO:0040011,  
894 P = 0.000037, n = 25 genes vs. 10 expected) and axon development (GO:0040011, P = 0.00043, n = 24 genes vs.  
895 11 expected) ontologies (first and third most significant ontology terms).  
896 Along with *unc-29* copies, 31 other genes exhibited a SNP with a decisive association with pyrantel resistance  
897 over that region, and five others lay between 80 and 83 Mbp (Table S11). In that latter region, a homolog of  
898 the aldicarb-resistant *fer-1* gene (Krajacic et al. 2013) (Fig. 5c) and a homolog of *chaf-1* homolog were also  
899 covered with a decisive SNP (Table 1, Fig. S17). Within the *fer-1* gene, two decisive and non-synonymous  
900 mutations (frameshift variants) were identified (Fig. 5c, S17). Of note, this region also encompassed a homolog  
901 of the beta-tubulin isotype-1 coding gene but the pervasive benzimidazole resistance across considered  
902 isolates rules out association with pyrantel sensitivity. To further prioritise candidate genes of functional  
903 interest, tissue enrichment analysis with the *C. elegans* homologs of this set of 37 genes found an over-  
904 representation of the anal depressor muscle in *C. elegans* (WBbt:0004292, fold-change = 8, q-value = 00055),  
905 defined by eight genes (*gsn1-1*, *rpl-24.1*, *rla-0*, *ddo-3*, *unc-29* and *yop-1* for the 47-53 Mbp QTL and *endu-1*,  
906 *nduf-7* for the downstream QTL region; Table 1).  
907 Because pyrantel is thought to disrupt cholinergic signalling at the neuro-muscular junction, we also inspected  
908 homologs of *C. elegans* genes (n = 106) known to be affected by aldicarb (an acetylcholinesterase inhibitor)  
909 and levamisole (an nAChR agonist), other than *unc-29* and *fer-1* already covered by decisive SNPs. This  
910 approach identified two homologs of genes whose mutation confers aldicarb hypersensitivity (Table 1), i.e.  
911 *dys-1* (aldicarb hypersensitive) located on chromosome 2 (18,840 bp away from the closest decisive SNP at  
912 49,510,860 and covered with five significant SNPs) and *erg-28* found on chromosome 1 (5,118 bp away from a  
913 decisive SNP at 87,813,389, Fig. 5c,d). On that chromosome, the narrow QTL region harboured seven genes,  
914 out of which an homolog of *dkf-2* also represents a likely candidate due to its ability to modulate sensitivity to  
915 aldicarb in some *C. elegans* genetic backgrounds (Sieburth et al. 2005). As a last candidate of interest, a *pqp-9*  
916 homolog - whose expression is modulated by pyrantel in the ascarid *Parascaris univalens* (Martin et al. 2020) -  
917 harboured 19 decisive SNPs that defined the QTL on chromosome 4 (Table 1, Fig. 5e,f, S17). Among these  
918 decisive SNPs, four defined major non-synonymous changes including a premature stop codon in exon 27 (SNP  
919 21,242,866 bp) thereby defining likely explanatory mutations. For these two QTL regions, however, genetic  
920 differentiation between modern isolates with known pyrantel sensitivity and the old worm isolate were not  
921 depart strongly from the genome average (Fig. S18, 19) and may be indicative of soft sweep in these regions.  
922 Across the decisive SNPs, the major reference allele (susceptible isolate) was not preferentially associated with  
923 higher pyrantel efficacy (52 out of the 97 SNPs; Fig. 5b,d,f, S19). In addition, allele frequency of the decisive  
924 variants falling within gene loci (n = 97) displayed absolute Pearson's *r* between 64.3 to 98.3% but missed the  
925 5% significance cut-off for 50 of them (P-value between 0.052 and 0.16) underscoring the effect of population  
926 structure in some cases. Of note, 28 of these SNPs were already segregating in the old worm isolate at a  
927 frequency compatible with their surmised sensitivity (Fig. S17). In the lack of preferential association of rare

Deleted: 19XIX<sup>th</sup> century

Formatted: Font: Italic

Deleted: -

Deleted: b

Deleted: a

Deleted: a

Deleted: laid

Deleted: an

Deleted:

Deleted: an

Deleted: n

Deleted: departing

939 alleles with sensitivity, the remaining SNPs have likely arisen over the last century (and they were not missed  
940 in the old worm isolate).

941 At the transcriptomic level, three-quarters of the genes harbouring one decisive SNP (n = 37 out of 97; Fig. 5g,  
942 S20) were differentially expressed between males and females collected upon pyrantel treatment, up-  
943 regulation in males being the rule in most cases (n = 27 genes) as seen for the most likely candidate genes (Fig.  
944 5g). Most candidate genes did not show significant differences in nucleotide diversity (FDR > 5%). However,  
945 slight deviations from the chromosome average were found over the *gsnl-1* ( $t_{27} = -2.19$ , nominal  $P = 0.038$ ) and  
946 *rpl-24.1* ( $t_{14} = -2.32$ , nominal  $P = 0.035$ ) in the pyrantel resistant isolates (Fig. S20).

947 Altogether, the SNPs found within a short list of five genes (*unc-29*, *chaf-1*, *endu-1*, *fer-1*, and *pgp-9*) define a  
948 set of robust genetic markers not affected by population structure.

### 950 Transcriptomic profiling of *Caenorhabditis elegans* lines selected for pyrantel resistance supports the 951 polygenic nature of this trait and gives support for highlighted candidate genes

952 To cross-validate the association signals found across field *C. nassatus* isolates, we compared the  
953 transcriptomic profiles of divergent *C. elegans* lines exposed to pyrantel or not for 12 generations. This data  
954 supported differential expression (adj.  $P < 0.05$ ) for ten out of the 14 genes identified within QTL regions (Fig.  
955 5j). However, a subset of 596 genes with higher fold-changes (Table S12) encompassed genes that defined  
956 significant enrichment for movement-related phenotypes (paralysis, q-value = 0.00021, or movement variant,  
957 q-value = 2.4e-06) and hypersensitivity to levamisole or nicotine (Table S13). The genes associated with  
958 hypersensitivity to these molecules were related to cuticle formation suggesting that permeability to the drug  
959 may be an indirect evasion strategy for the worms.

## 960 Discussion

961 This work delivers the first resolution of any cyathostomin genomes and provides the first genomic landscape  
962 of pyrantel resistance in any parasitic nematodes. We also gained insights into the temporal evolution of  
963 genome-wide diversity in *C. nassatus* over the past 150 years.

964 Whole-genome-based evolutionary analysis found that *C. nassatus* was a closer relative of Ancylostomatidae  
965 than the Trichostrongyloidea as already reported using the *C. goldi* proteome (International Helminth Genomes  
966 2019). Similar to *A. ceylanicum* (Merchant et al. 2022), the *C. nassatus* genome harboured active endogenous  
967 viral elements that had distinct transcriptional patterns across sexes. It remains unknown however whether  
968 sexual metabolism affects their expression or if they play an active role in defining sexual traits. The similarity  
969 with Ancylostomatidae did not apply to their genome size which was about twice as large for *C. nassatus* as for  
970 *A. ceylanicum* (Ancylostomatidae, 313 Mbp) (Schwarz et al. 2015) but matched the 614-Mbp genome of  
971 *Teladorsagia circumcincta* (Trichostrongylidae) (Hassan et al. 2023). This difference in genome size matched a  
972 significant expansion of transposon elements that has been encountered across other helminth genomes  
973 (International Helminth Genomes 2019). Of note, transposons were contained to the edge of the X  
974 chromosome arms, which might suggest limited colonisation and a recent differentiation of that chromosome,  
975 although the abundance of transposons in the sex chromosome is a poor correlate of evolutionary times in a  
976 wide range of species (Matsubara et al. 2006; Chalopin et al. 2015).

977 Access to past worm material offered an opportunity to track the evolution of genetic diversity in the past  
978 century for *C. nassatus*. The pattern of rare variant sharing would favour significant connectivity between old  
979 Egyptian worms and modern Western populations. However, this pattern was more pronounced with the  
980 Ukrainian isolates that seem to have contributed to every other isolate diversity in more recent times. This  
981 pattern was also found in the reconstructed admixture graph, although the surmised important extent of gene  
982 flow between parasite populations due to horse movement and the relatively limited size of the population set  
983 may have obscured this analysis (Patterson et al. 2012; Gautier et al. 2022). The origin of Cyathostominae  
984 remains unknown to date but they encompass a wide range of hosts including wild equids (Lichtenfels et al.  
985 2008; Kuzmina et al. 2009, 2013, 2020; Tombak et al. 2021) and elephants (Chel et al. 2020). Their parasitic  
986 mode of life would hence suggest shared tracks of history with their hosts. In this respect, additional sampling  
987 of *C. nassatus* isolates along the road of horse domestication routes could confirm the contribution of  
988

Deleted: it is likely that the remaining SNPs have

Deleted: that

Deleted: three

Deleted: -

Deleted: and whose contribution to pyrantel resistance can be reproduced in independent another organism

Deleted: would

Deleted: genome

Deleted: that

Deleted: larger

Deleted: than

Deleted: (Ancylostomatidae, 313 Mbp)

Deleted: (Trichostrongylidae)

Deleted: s

Deleted: even

Deleted: s

Deleted: s

Deleted: also applied

1007 contemporary horse expansion from the lower Volga-Don region (Librado et al. 2021) to the building of current  
1008 *C. nassatus* populations. Access to horse coprolites would be key to sampling more ancient times as illustrated  
1009 for middle-age dated *Trichuris trichiura* (Doyle, Søe, et al. 2022). Additional genetic profiling of isolates from  
1010 wild African equids could also support the importance of horse domestication and management in the  
1011 population structure of this species.

1012 Similar to observations made between ancient and modern *T. trichiura* (Doyle, Søe, et al. 2022), lower,  
1013 nucleotide diversity was found in contemporary isolates relative to old North African *C. nassatus* individuals.  
1014 In that respect, additional sampling efforts from contemporary North African worms would help resolve the  
1015 temporal and geographical contributions to the observed contrast in nucleotide diversity. Of note, the most  
1016 important genetic differentiation occurred over pyrantel-resistance-associated regions supporting the  
1017 contribution of modern anthelmintic treatments in reshaping global parasite diversity. In this respect, the  
1018 mapping of pyrantel resistance Quantitative Trait Loci (QTL) highlighted a few distinct regions among which a  
1019 functional hub in the middle of chromosome 2 dominated. In this region, *unc-29* was the only known functional  
1020 candidate already associated with pyrantel resistance. Our data, however, widen the previous picture with  
1021 other mutations found within genes affecting cholinergic signalling either through regulation of receptors  
1022 distribution at the synapse (*dys-1*), the regulation of cholinergic signalling including *fer-1* (Krajacic et al. 2013),  
1023 *dkf-2* (Sieburth et al. 2005), and *chaf-1* (Gottschalk et al. 2005), or an *erg-28* homolog that is required for the  
1024 function of the potassium SLO-1 channels (Cheung et al. 2020), the targets of emodepside (Welz et al. 2011).  
1025 As such, the mechanistic landscape becomes more complex, as it remains to determine if a single mutation in  
1026 any of these genes is sufficient or necessary to affect pyrantel resistance and if so, what mutation occurred  
1027 first and what compensatory mutations may be needed. The broad QTL region identified would suggest at least  
1028 that these candidates belong to a genomic hub that is less prone to recombination. Further investigation  
1029 abrogating the function of the identified candidate genes within different genetic knock-out backgrounds, as  
1030 applied for the study of aldicarb resistance (Sieburth et al. 2005), would contribute to disentangling the relative  
1031 importance of each gene to the phenotype of interest while reconstructing the matrix of epistatic interactions  
1032 between the proposed candidates.

1033 Among the list of candidates identified in the QTL regions, *unc-29* was the only known functional candidate  
1034 already associated with pyrantel resistance while the role of *pyp-9* was corroborated in *Parascaris univalens*  
1035 exposed to pyrantel (Martin et al. 2020). However, *unc-38* seems to be ruled out in *C. nassatus* and the  
1036 contribution of *unc-63* remains uncertain as a few SNP were associated with pyrantel resistance in the locus  
1037 vicinity. While the associated SNPs certainly define a set of markers to be tested for monitoring of field  
1038 cyathostomin isolates, the high number of SNPs reaching significance and the large number of differentially  
1039 expressed genes in selected *C. elegans* lines would be compatible with a polygenic architecture for pyrantel  
1040 resistance.

1041 Of note, the close vicinity between the beta-tubulin locus that is known to affect benzimidazole resistance in  
1042 cyathostomin (Kwa et al. 1995; Hodgkinson et al. 2008) or other nematode species (Sallé et al. 2019), and  
1043 pyrantel-associated QTL may result in linked selection over that region by any of these two drugs. Under the  
1044 assumption of conserved synteny between *C. nassatus* and *A. ceylanicum*, this genomic proximity may  
1045 underpin the previously described synergistic effect of pyrantel and the pro-benzimidazole drug febantel in the  
1046 management of *A. ceylanicum* (Hopkins and Gyr 1991).

1047 This detailed resolution sheds light on a complex network of genes whose function in the regulation of  
1048 cholinergic signalling or the regulation of other drug targets opens novel perspectives for the use of drug  
1049 combination in the field.

1050  
1051  
1052  
1053

Formatted: Font: Italic

Deleted: *i*

Deleted: significant loss of

Formatted: Font: Italic

Deleted: effort

Deleted: north

Deleted: occurred over the past 150 years in *C. nassatus*. tT

Deleted: resistance

Deleted: complexifies

Formatted: Font: Italic

Deleted: -

Deleted: -

Deleted: a

1064  
1065  
1066  
1067  
1068

### Acknowledgements

The authors are greatly indebted to the breeders who granted access to their facilities and horses for sample collection in Normandy.

1069

### Data, scripts, code, and supplementary information availability

1070 The raw sequencing data have been submitted to the European Nucleotide Archive under study  
1071 accession PRJEB63274. The HiFi reads and Hi-C data generated for *C. nassatus* are deposited with accession  
1072 ERS15765218 and ERS15765233, while HiFi data generated for *Coronocyclus labiatus*, *Cyathostomum*  
1073 *catinatum*, *Cylicostephanus goldi*, *Cylicostephanus longibursatus* and *Cylicocyclus insigne* correspond to  
1074 accessions ERS15970850, ERS15970852, ERS15970851, ERS15978829, ERS15970849 respectively.

1075 Scripts and code are available online: <https://doi.org/10.57745/1FB3SD>.

1076 Supplementary information is available online: <https://doi.org/10.57745/1FB3SD>.

1077  
1078

1079

### Conflict of interest disclosure

1080 The authors declare that they comply with the PCI rule of having no financial conflicts of interest in relation  
1081 to the content of the article.

1082

1083

### Funding

1084 This project was funded by the French [Horse](#) and [Horse Riding Institute](#) (IFCE) and the Fonds Éperon.  
1085 MGX and Get-PlaGe (doi:10.17180/nvxj-533) acknowledge financial support from France Génomique National  
1086 infrastructure, funded as part of [the](#) "Investissement d'Avenir" program managed by Agence Nationale pour la  
1087 Recherche (contract ANR-10-INBS-09)." [The participation of T. A. Kuzmina in this study was partially supported](#)  
1088 [by the EU NextGenerationEU through the Recovery and Resilience Plan for Slovakia; projects No. 09I03-03-](#)  
1089 [V01-00015](#).

1090

Deleted: horse

Deleted: horse riding institute

## References

- 1093  
1094  
1095 Alexa A. 2016. topGO: Enrichment Analysis for Gene Ontology.  
1096 Anon. 2019. Picard toolkit. Available from: <https://broadinstitute.github.io/picard/>  
1097 Anjos DHDS, Rodrigues MDLA. 2006. Diversity of the infracommunities of strongylid nematodes in the ventral  
1098 colon of *Equus caballus* from Rio de Janeiro state, Brazil. *Veterinary Parasitology* 136: 251– 257  
1099 Antonopoulos A, Doyle SR, Bartley DJ, Morrison AA, Kaplan R, Howell S, Neveu C, Busin V, Devaney E, Laing R.  
1100 2022. Allele specific PCR for a major marker of levamisole resistance in *Haemonchus contortus*. *Int J*  
1101 *Parasitol Drugs Drug Resist* 20:17–26.  
1102 Bellaw JL, Nielsen MK (2020) Meta-analysis of cyathostomin species-specific prevalence and relative  
1103 abundance in domestic horses from 1975-2020: emphasis on geographical region and specimen  
1104 collection method. *Parasite & Vectors* 13(1):509.  
1105 Benson G. 1999. Tandem repeats finder: a program to analyze DNA sequences. *Nucleic Acids Res* 27:573–580.  
1106 Blanchard A, Guegnard F, Charvet CL, Crisford A, Courtot E, Sauve C, Harmache A, Duguet T, O'Connor V,  
1107 Castagnone-Sereno P, et al. 2018. Deciphering the molecular determinants of cholinergic  
1108 anthelmintic sensitivity in nematodes: When novel functional validation approaches highlight major  
1109 differences between the model *Caenorhabditis elegans* and parasitic species. *PLoS Pathog*  
1110 14:e1006996.  
1111 Boisseau M, Dhone-Pollet S, Bars-Cortina D, Courtot É, Serreau D, Annonay G, Lluch J, Gesbert A, Reigner F,  
1112 Sallé G, et al. 2023. Species interactions, stability, and resilience of the gut microbiota - helminth  
1113 assemblage in horses. *iScience*:106044.  
1114 Bradley M, Taylor R, Jacobson J, Guex M, Hopkins A, Jensen J, Leonard L, Waltz J, Kuykens L, Sow PS, et al.  
1115 2021. Medicine donation programmes supporting the global drive to end the burden of neglected  
1116 tropical diseases. *Transactions of The Royal Society of Tropical Medicine and Hygiene* 115:136–144.  
1117 Bucknell DG, Gasser RB, Beveridge I. 1995. The prevalence and epidemiology of gastrointestinal parasites of  
1118 horses in Victoria, Australia. *Int J Parasitol* 25:711–724.  
1119 Campbell MS, Holt C, Moore B, Yandell M. 2014. Genome Annotation and Curation Using MAKER and MAKER-  
1120 P. *CP in Bioinformatics* [Internet] 48. Available from:  
1121 <https://onlinelibrary.wiley.com/doi/10.1002/0471250953.bi0411s48>  
1122 Chalopin D, Volff J-N, Galiana D, Anderson JL, Schartl M. 2015. Transposable elements and early evolution of  
1123 sex chromosomes in fish. *Chromosome Res* 23:545–560.  
1124 Chel HM, Iwaki T, Hmoon MM, Thaw YN, Soe NC, Win SY, Bawm S, Htun LL, Win MM, Oo ZM, et al. 2020.  
1125 Morphological and molecular identification of cyathostomine gastrointestinal nematodes of  
1126 Murshidia and Quilonia species from Asian elephants in Myanmar. *Int J Parasitol Parasites Wildl*  
1127 11:294–301.  
1128 Cheng H, Concepcion GT, Feng X, Zhang H, Li H. 2021. Haplotype-resolved de novo assembly using phased  
1129 assembly graphs with hifiasm. *Nat Methods*, 18:170–175.  
1130 Cheung TP, Choe J-Y, Richmond JE, Kim H. 2020. BK channel density is regulated by endoplasmic reticulum  
1131 associated degradation and influenced by the SKN-1A/NRF1 transcription factor. Hart AC, editor. *PLoS*  
1132 *Genet* 16:e1008829.  
1133 Collobert-Laugier C, Hoste H, Sevin C, Dorchies P. 2002. Prevalence, abundance and site distribution of equine  
1134 small strongyles in Normandy, France. *Vet Parasitol* 110:77–83.  
1135 Cotton JA, Bennuru S, Grote A, Harsha B, Tracey A, Beech R, Doyle SR, Dunn M, Hotopp JCD, Holroyd N, et al.  
1136 2017. The genome of *Onchocerca volvulus*, agent of river blindness. *Nat Microbiol* 2:16216.  
1137 Courtot É, Boisseau M, Dhone-Pollet S, Serreau D, Gesbert A, Reigner F, Basiaga M, Kuzmina T, Lluch J,  
1138 Annonay G, et al. 2023. Comparison of two molecular barcodes for the study of equine strongylid  
1139 communities with amplicon sequencing. *PeerJ* 11:e15124.  
1140 Courtot E, Charvet CL, Beech RN, Harmache A, Wolstenholme AJ, Holden-Dye L, O'Connor V, Peineau N,  
1141 Woods DJ, Neveu C. 2015. Functional Characterization of a Novel Class of Morantel-Sensitive  
1142 Acetylcholine Receptors in Nematodes. Aroian RV, editor. *PLoS Pathog* 11:e1005267.

Deleted: <https://broadinstitute.github.io/picard/>

Formatted: Font: Italic

Formatted: Font: Italic

Field Code Changed

- 1144 Cwiklinski K, Merga JY, Lake SL, Hartley C, Matthews JB, Paterson S, Hodgkinson JE. 2013. Transcriptome  
 1145 analysis of a parasitic clade V nematode: comparative analysis of potential molecular anthelmintic  
 1146 targets in *Cylicostephanus goldi*. *Int J Parasitol* 43:917–927.
- 1147 [Delcher AL, Phillippy A, Carlton J, Salzberg SL. 2002. Fast algorithms for large-scale genome alignment and](#)  
 1148 [comparison. \*Nucleic Acids Res\* 30:2478–2483](#)
- 1149 Doyle SR. 2022. Improving helminth genome resources in the post-genomic era. *Trends in Parasitology*  
 1150 38:831–840.
- 1151 Doyle SR, Illingworth CJR, Laing R, Bartley DJ, Redman E, Martinelli A, Holroyd N, Morrison AA, Rezansoff A,  
 1152 Tracey A, et al. 2019. Population genomic and evolutionary modelling analyses reveal a single major  
 1153 QTL for ivermectin drug resistance in the pathogenic nematode, *Haemonchus contortus*. *BMC*  
 1154 *Genomics* 20:218.
- 1155 Doyle SR, Laing R, Bartley D, Morrison A, Holroyd N, Maitland K, Antonopoulos A, Chaudhry U, Flis I, Howell S,  
 1156 et al. 2022. Genomic landscape of drug response reveals mediators of anthelmintic resistance. *Cell*  
 1157 *Reports* 41:111522.
- 1158 Doyle SR, Sjøe MJ, Nejsum P, Betson M, Cooper PJ, Peng L, Zhu X-Q, Sanchez A, Matamoros G, Sandoval GAF,  
 1159 et al. 2022. Population genomics of ancient and modern *Trichuris trichiura*. *Nat Commun* 13:3888.
- 1160 Doyle SR, Tracey A, Laing R, Holroyd N, Bartley D, Bazant W, Beasley H, Beech R, Britton C, Brooks K, et al.  
 1161 2020. Genomic and transcriptomic variation defines the chromosome-scale assembly of *Haemonchus*  
 1162 *contortus*, a model gastrointestinal worm. *Commun Biol* 3:656.
- 1163 Dudchenko O, Batra SS, Omer AD, Nyquist SK, Hoeger M, Durand NC, Shamim MS, Machol I, Lander ES, Aiden  
 1164 AP, et al. 2017. De novo assembly of the *Aedes aegypti* genome using Hi-C yields chromosome-length  
 1165 scaffolds. *Science* 356:92–95.
- 1166 Durand NC, Robinson JT, Shamim MS, Machol I, Mesirov JP, Lander ES, Aiden EL. 2016. Juicebox Provides a  
 1167 Visualization System for Hi-C Contact Maps with Unlimited Zoom. *Cell Syst* 3:99–101.
- 1168 Durand NC, Shamim MS, Machol I, Rao SSP, Huntley MH, Lander ES, Aiden EL. 2016. Juicer Provides a One-  
 1169 Click System for Analyzing Loop-Resolution Hi-C Experiments. *Cell Syst* 3:95–98.
- 1170 Durrant C, Thiele EA, Holroyd N, Doyle SR, Sallé G, Tracey A, Sankaranarayanan G, Lotkowska ME, Bennett  
 1171 HM, Huckvale T, et al. 2020. Population genomic evidence that human and animal infections in Africa  
 1172 come from the same populations of *Draacunculus medinensis*. Basáñez M-G, editor. *PLOS Neglected*  
 1173 *Tropical Diseases* 14:e0008623.
- 1174 Emms DM, Kelly S. 2019. OrthoFinder: phylogenetic orthology inference for comparative genomics. *Genome*  
 1175 *Biol* 20:238.
- 1176 Ferretti L, Ramos-Onsins SE, Pérez-Enciso M. 2013. Population genomics from pool sequencing. *Mol Ecol*  
 1177 22:5561–5576.
- 1178 Flynn JM, Hubley R, Goubert C, Rosen J, Clark AG, Feschotte C, Smit AF. 2020. RepeatModeler2 for automated  
 1179 genomic discovery of transposable element families. *Proc. Natl. Acad. Sci. U.S.A.* 117:9451–9457.
- 1180 G. B. D. DALYs, Hale Collaborators. 2017. Global, regional, and national disability-adjusted life-years (DALYs)  
 1181 for 333 diseases and injuries and healthy life expectancy (HALE) for 195 countries and territories,  
 1182 1990-2016: a systematic analysis for the Global Burden of Disease Study 2016. *Lancet* 390:1260–  
 1183 1344.
- 1184 Gamba C, Hanghøj K, Gaunitz C, Alfarhan AH, Alquraishi SA, Al-Rasheid KAS, Bradley DG, Orlando L. 2016.  
 1185 Comparing the performance of three ancient DNA extraction methods for high-throughput  
 1186 sequencing. *Mol Ecol Resour* 16:459–469.
- 1187 Gandasegui J, Onwuchekwa C, Krolewiecki AJ, Doyle SR, Pullan RL, Enbiale W, Kepha S, Hatherell HA, van  
 1188 Lieshout L, Cambra-Pellejà M, et al. 2022. Ivermectin and albendazole coadministration:  
 1189 opportunities for strongyloidiasis control. *Lancet Infect Dis* 22:e341–e347.
- 1190 Gao Y, Qiu J-H, Zhang B-B, Su X, Fu X, Yue D-M, Wang C-R. 2017. Complete mitochondrial genome of parasitic  
 1191 nematode *Cylicocyclus nassatus* and comparative analyses with *Cylicocyclus insigne*. *Exp Parasitol*  
 1192 172:18–22.
- 1193 Gautier M. 2015. Genome-Wide Scan for Adaptive Divergence and Association with Population-Specific

Formatted: Font: Italic

1194 Covariates. *Genetics* 201:1555–1579.

1195 Gautier M, Vitalis R, Flori L, Estoup A. 2022. *f*-Statistics estimation and admixture graph construction with  
1196 Pool-Seq or allele count data using the R package *poolfstat*. *Molecular Ecology Resources* 22:1394–  
1197 1416.

1198 Gottschalk A, Almedom RB, Schedletzky T, Anderson SD, Yates JR, Schafer WR. 2005. Identification and  
1199 characterization of novel nicotinic receptor-associated proteins in *Caenorhabditis elegans*. *EMBO J*  
1200 24:2566–2578.

1201 Gurevich A, Saveliev V, Vyahhi N, Tesler G. 2013. QUAST: quality assessment tool for genome assemblies.  
1202 *Bioinformatics* 29:1072–1075.

1203 Han MV, Thomas GWC, Lugo-Martinez J, Hahn MW. 2013. Estimating gene gain and loss rates in the presence  
1204 of error in genome assembly and annotation using CAFE 3. *Mol Biol Evol* 30:1987–1997.

1205 Hart AJ, Ginzburg S, Xu M (Sam), Fisher CR, Rahmatpour N, Mitton JB, Paul R, Wegrzyn JL. 2020. EnTAP :  
1206 Bringing faster and smarter functional annotation to non-model eukaryotic transcriptomes. *Mol Ecol*  
1207 *Resour* 20:591–604.

1208 Hassan SU, Chua EG, Paz EA, Tay CY, Greeff JC, Palmer DG, Dudchenko O, Aiden EL, Martin GB, Kaur P. 2023.  
1209 Chromosome-length genome assembly of *Teladorsagia circumcincta* – a globally important helminth  
1210 parasite in livestock. *BMC Genomics* 24:74.

1211 Herd RP. 1990. The changing world of worms: the rise of the cyathostomes and the decline of *Strongylus*  
1212 *vulgaris*. *Compendium on Continuing Education for the Practicing Veterinarian* 12:732–734.

1213 Hernández-Plaza A, Szklarczyk D, Botas J, Cantalapiedra CP, Giner-Lamia J, Mende DR, Kirsch R, Rattei T,  
1214 Letunic I, Jensen LJ, et al. 2023. eggNOG 6.0: enabling comparative genomics across 12 535  
1215 organisms. *Nucleic Acids Res* 51:D389–D394.

1216 Hodgkinson JE, Clark HJ, Kaplan RM, Lake SL, Matthews JB. 2008. The role of polymorphisms at beta tubulin  
1217 isotype 1 codons 167 and 200 in benzimidazole resistance in cyathostomins. *Int J Parasitol* 38:1149–  
1218 1160.

1219 Hoff KJ, Lomsadze A, Borodovsky M, Stanke M. 2019. Whole-Genome Annotation with BRAKER. In: Kollmar  
1220 M, editor. Gene Prediction. Vol. 1962. Methods in Molecular Biology. New York, NY: Springer New  
1221 York. p. 65–95. Available from: [http://link.springer.com/10.1007/978-1-4939-9173-0\\_5](http://link.springer.com/10.1007/978-1-4939-9173-0_5)

1222 Hopkins TJ, Gyr P. 1991. Synergism of a combination of febantel and pyrantel embonate against *Ancylostoma*  
1223 *caninum* on dogs. *Vet Med Rev*.

1224 International Helminth Genomes C. 2019. Comparative genomics of the major parasitic worms. *Nat Genet*  
1225 51:163–174.

1226 Jenkins E, Backwell A-L, Bellow J, Colpitts J, Liboiron A, McRuer D, Mediil S, Parker S, Shury T, Smith M, et al.  
1227 2020. Not playing by the rules: Unusual patterns in the epidemiology of parasites in a natural  
1228 population of feral horses (*Equus caballus*) on Sable Island, Canada. *International Journal for*  
1229 *Parasitology: Parasites and Wildlife* 11:183–190.

1230 Jürgenschellert L, Krücken J, Bousquet E, Bartz J, Heyer N, Nielsen MK, von Samson-Himmelstjerna G. 2022.  
1231 Occurrence of Strongylid Nematode Parasites on Horse Farms in Berlin and Brandenburg, Germany,  
1232 With High Seroprevalence of *Strongylus vulgaris* Infection. *Front Vet Sci* 9:892920.

1233 Kaplan RM, Vidyashankar AN. 2012. An inconvenient truth: Global worming and anthelmintic resistance. *Vet*  
1234 *Parasitol* 186:70–78.

1235 Kingan SB, Heaton H, Cudini J, Lambert CC, Baybayan P, Galvin BD, Durbin R, Korlach J, Lawniczak MKN. 2019.  
1236 A High-Quality De novo Genome Assembly from a Single Mosquito Using PacBio Sequencing. *Genes*  
1237 (*Basel*) 10.

1238 Kopp SR, Coleman GT, Traub RJ, McCarthy JS, Kotze AC. 2009. Acetylcholine receptor subunit genes from  
1239 *Ancylostoma caninum*: Altered transcription patterns associated with pyrantel resistance.  
1240 *International Journal for Parasitology* 39:435–441.

1241 Kopp SR, Kotze AC, McCarthy JS, Traub RJ, Coleman GT. 2008. Pyrantel in small animal medicine: 30 years on.  
1242 *The Veterinary Journal* 178:177–184.

1243 Krajacic P, Pistilli EE, Tanis JE, Khurana TS, Lamitina ST. 2013. FER-1/Dysferlin promotes cholinergic signaling

Formatted: Font: Italic

Formatted: Font: Italic

Formatted: Font: Italic

Formatted: Font: Italic

1244 at the neuromuscular junction in *C. elegans* and mice. *Biology Open* 2:1245–1252.

1245 [Kuzmina T, Kuzmin Y \(2008\) The strongylid community of working donkeys \(\*Equus asinus\* L.\) in Ukraine.](#)

1246 [Vestnik Zoologii 42\(2\):99–104.](#)

1247 [Kuzmina TA, Zvegintsova NS, Zharkikh TL \(2009\) Strongylid community structure of the Przewalski's horses](#)

1248 [\(\*Equus ferus przewalskii\*\) from the Biosphere Reserve "Askania-Nova", Ukraine. \*Vestnik zoologii\*, 43](#)

1249 [\(3\). 209–215.](#)

1250 Kuzmina T. 2012. Analysis of Regional Peculiarities of Strongylid (Nematoda, Strongylidae) Biodiversity in

1251 Domestic Horses in Ukraine. *Vestnik Zoologii* 46: 9–17.

1252 [Kuzmina TA, Kharchenko VA, Zvegintsova NS, Zhang L, Liu J \(2013\) Strongylids \(Nematoda: Strongylidae\) in](#)

1253 [two zebra species from the "Askania-Nova" Biosphere Reserve, Ukraine: biodiversity and parasite](#)

1254 [community structure. \*Helminthologia\* 50:172–180.](#)

1255 Kuzmina T, Holovachov O. 2023. Equine Strongylidae and other parasitic nematodes described by Arthur

1256 Looss during 1895–1911 in the collections of the Swedish Museum of Natural History. *Zootaxa*

1257 5227:151–193.

1258 Kuzmina TA, Dzeverin I, Kharchenko VA. 2016. Strongylids in domestic horses: Influence of horse age, breed

1259 and deworming programs on the strongyle parasite community. *Vet Parasitol* 227:56–63.

1260 Kuzmina TA, Zvegintsova NS, Yasynetska NI, Kharchenko VA. 2020. Anthelmintic resistance in strongylids

1261 (Nematoda: Strongylidae) parasitizing wild and domestic equids in the Askania Nova Biosphere

1262 Reserve, Ukraine. *Ann Parasitol* 66:49–60.

1263 Kwa MS, Kooyman FN, Boersema JH, Roos MH. 1993. Effect of selection for benzimidazole resistance in

1264 *Haemonchus contortus* on beta-tubulin isotype 1 and isotype 2 genes. *Biochem Biophys Res Commun*

1265 191:413–419.

1266 Kwa MS, Veenstra JG, Van Dijk M, Roos MH. 1995. Beta-tubulin genes from the parasitic nematode

1267 *Haemonchus contortus* modulate drug resistance in *Caenorhabditis elegans*. *J Mol Biol* 246:500–510.

1268 Laing R, Doyle SR, McIntyre J, Maitland K, Morrison A, Bartley DJ, Kaplan R, Chaudhry U, Sargison N, Tait A, et

1269 al. 2022. Transcriptomic analyses implicate neuronal plasticity and chloride homeostasis in

1270 ivermectin resistance and response to treatment in a parasitic nematode. Andersen EC, editor. *PLoS*

1271 *Pathog* 18:e1010545.

1272 Laing R, Gillan V, Devaney E. 2017. Ivermectin - Old Drug, New Tricks? *Trends Parasitol* 33:463–472.

1273 Lee RYN, Howe KL, Harris TW, Arnaboldi V, Cain S, Chan J, Chen WJ, Davis P, Gao S, Grove C, et al. 2018.

1274 WormBase 2017: molting into a new stage. *Nucleic Acids Res* 46:D869–D874.

1275 Letunic I, Bork P. 2021. Interactive Tree Of Life (iTOL) v5: an online tool for phylogenetic tree display and

1276 annotation. *Nucleic Acids Research* 49:W293–W296.

1277 Li H. 2018. Minimap2: pairwise alignment for nucleotide sequences. Birol I, editor. *Bioinformatics* 34:3094–

1278 3100.

1279 Librado P, Khan N, Fages A, Kusliy MA, Suchan T, Tonasso-Calvière L, Schiavinato S, Alioglu D, Fromentier A,

1280 Perdereau A, et al. 2021. The origins and spread of domestic horses from the Western Eurasian

1281 steppes. *Nature* 598:634–640.

1282 Lichtenfels JR, Kharchenko VA, Dvojnjos GM. 2008. Illustrated identification keys to strongylid parasites

1283 (Strongylidae: Nematoda) of horses, zebras and asses (Equidae). *Vet Parasitol* 156:4–161.

1284 [Louro M, Kuzmina TA, Bredtmann CM, Diekmann I, de Carvalho LMM, von Samson-Himmelstjerna G, Krücken](#)

1285 [J \(2021\) Genetic variability, cryptic species and phylogenetic relationship of six cyathostomin species](#)

1286 [based on mitochondrial and nuclear sequences. \*Scientific Reports\* 11\(1\):8245.](#)

1287 Love MI, Huber W, Anders S. 2014. Moderated estimation of fold change and dispersion for RNA-seq data

1288 with DESeq2. *Genome Biol* 15:550.

1289 Luu K, Bazin E, Blum MGB. 2017. *pcadapt* : an R package to perform genome scans for selection based on

1290 principal component analysis. *Mol Ecol Resour* 17:67–77.

1291 Lyons E. 2003. Population-S benzimidazole- and tetrahydropyrimidine-resistant small strongyles in a pony

1292 herd in Kentucky (1977-1999): effects of anthelmintic treatment on the parasites as determined in

1293 critical tests. *Parasitol Res* 91:407–411.

Deleted: e-7

Deleted: e-15

Formatted: Font: Italic

Formatted: Font: Italic

Formatted: Font: Italic

Deleted: ¶

1297 Lyons ET, Drudge JH, Tolliver SC. 1992. Review of prevalence surveys of internal parasites recovered (1951-  
1298 1990) from horses at necropsy in Kentucky. *Journal of Equine Veterinary Science* 12:9–16.

1299 Lyons ET, Tolliver SC, Drudge JH. 1999. Historical perspective of cyathostomes: prevalence, treatment and  
1300 control programs. *Vet Parasitol* 85:97–111; discussion 111-2, 215–225.

1301 Malsa J, Courtot É, Boisseau M, Dumont B, Gombault P, Kuzmina TA, Basiaga M, Lluch J, Annonay G, Dhone-  
1302 Pollet S, et al. 2022. Effect of sainfoin (*Onobrychis viciifolia*) on cyathostomin eggs excretion, larval  
1303 development, larval community structure and efficacy of ivermectin treatment in horses.  
1304 *Parasitology* 149:1439–1449.

1305 Marini F, Ludt A, Linke J, Strauch K. 2021. GeneTonic: an R/Bioconductor package for streamlining the  
1306 interpretation of RNA-seq data. *BMC Bioinformatics* 22:610.

1307 Marsh AE, Lakritz J. 2023. Reflecting on the past and fast forwarding to present day anthelmintic resistant  
1308 *Ancylostoma caninum* - A critical issue we neglected to forecast. *Int J Parasitol Drugs Drug Resist*  
1309 22:36–43.

1310 Martin F, Dube F, Karlsson Lindsjö O, Eydal M, Höglund J, Bergström TF, Tydén E. 2020. Transcriptional  
1311 responses in *Parascaris univalens* after in vitro exposure to ivermectin, pyrantel citrate and  
1312 thiabendazole. *Parasites Vectors* 13:342.

1313 Matsubara K, Tarui H, Toriba M, Yamada K, Nishida-Umehara C, Agata K, Matsuda Y. 2006. Evidence for  
1314 different origin of sex chromosomes in snakes, birds, and mammals and step-wise differentiation of  
1315 snake sex chromosomes. *Proc. Natl. Acad. Sci. U.S.A.* 103:18190–18195.

1316 McKenna A, Hanna M, Banks E, Sivachenko A, Cibulskis K, Kernytzky A, Garimella K, Altshuler D, Gabriel S,  
1317 Daly M, et al. 2010. The Genome Analysis Toolkit: a MapReduce framework for analyzing next-  
1318 generation DNA sequencing data. *Genome Res* 20:1297–1303.

1319 Merchant M, Mata CP, Liu Y, Zhai H, Protasio AV, Modis Y. 2022. A bioactive phlebovirus-like envelope  
1320 protein in a hookworm endogenous virus. *Sci Adv* 8:eabj6894.

1321 Mistry J, Chuguransky S, Williams L, Qureshi M, Salazar GA, Sonnhammer ELL, Tosatto SCE, Paladin L, Raj S,  
1322 Richardson LJ, et al. 2021. Pfam: The protein families database in 2021. *Nucleic Acids Research*  
1323 49:D412–D419.

1324 Morgulis A, Gertz EM, Schäffer AA, Agarwala R. 2006. A fast and symmetric DUST implementation to mask  
1325 low-complexity DNA sequences. *J Comput Biol* 13:1028–1040.

1326 Moser W, Schindler C, Keiser J. 2017. Efficacy of recommended drugs against soil transmitted helminths:  
1327 systematic review and network meta-analysis. *BMJ* 358:j4307.

1328 Neveu C, Charvet CL, Fauvin A, Cortet J, Beech RN, Cabaret J. 2010. Genetic diversity of levamisole receptor  
1329 subunits in parasitic nematode species and abbreviated transcripts associated with resistance.  
1330 *Pharmacogenet Genomics* 20:414–425.

1331 Nielsen MK. 2022. Anthelmintic resistance in equine nematodes: Current status and emerging trends. *Int J*  
1332 *Parasitol Drugs Drug Resist* 20:76–88.

1333 Nielsen MK, Steuer AE, Anderson HP, Gavrilic S, Carpenter AB, Redman EM, Gilleard JS, Reinemeyer CR,  
1334 Poissant J. 2022. Shortened egg reappearance periods of equine cyathostomins following ivermectin  
1335 or moxidectin treatment: morphological and molecular investigation of efficacy and species  
1336 composition. *Int J Parasitol* 52:787–798.

1337 Ogbourne CP. 1972. Observations on the free-living stages of strongylid nematodes of the horse. *Parasitology*  
1338 64:461–477.

1339 Patro R, Duggal G, Love MI, Irizarry RA, Kingsford C. 2017. Salmon provides fast and bias-aware quantification  
1340 of transcript expression. *Nat. Methods* 14:417–419.

1341 Patterson N, Moorjani P, Luo Y, Mallick S, Rohland N, Zhan Y, Genschoreck T, Webster T, Reich D. 2012.  
1342 Ancient admixture in human history. *Genetics* 192:1065–1093.

1343 Paysan-Lafosse T, Blum M, Chuguransky S, Grego T, Pinto BL, Salazar GA, Bileschi ML, Bork P, Bridge A,  
1344 Colwell L, et al. 2023. InterPro in 2022. *Nucleic Acids Res* 51:D418–D427.

1345 Pfaffinger PJ, Cushman SJ, Nanao MH, Jahng AW, DeRubeis D, Choe S. 2000. Voltage dependent activation of  
1346 potassium channels is coupled to T1 domain structure. *Nat. Struct Biol.* 7:403–407.

Formatted: French

Field Code Changed

Formatted: French

Field Code Changed

Formatted: French

Formatted: French

Field Code Changed

Formatted: Font: Italic

Formatted: Font: Italic

Field Code Changed

Field Code Changed

1347 Poissant J, Gavriluc S, Bellaw J, Redman EM, Avramenko RW, Robinson D, Workentine ML, Shury TK, Jenkins  
1348 EJ, McLoughlin PD, et al. 2021. A repeatable and quantitative DNA metabarcoding assay to  
1349 characterize mixed strongyle infections in horses. *Int J Parasitol* 51:183–192.

1350 Raineri E, Ferretti L, Esteve-Codina A, Nevado B, Heath S, Pérez-Enciso M. 2012. SNP calling by sequencing  
1351 pooled samples. *BMC Bioinformatics* 13:239.

1352 Robertson AP, Bjørn HE, Martin RJ. 2000. Pyrantel resistance alters nematode nicotinic acetylcholine receptor  
1353 single-channel properties. *Eur J Pharmacol* 394:1–8.

1354 Robertson SJ, Pennington AJ, Evans AM, Martin RJ. 1994. The action of pyrantel as an agonist and an open  
1355 channel blocker at acetylcholine receptors in isolated *Ascaris suum* muscle vesicles. *Eur J Pharmacol*  
1356 271:273–282.

1357 Sallé G, Cortet J, Bois I, Dubes C, Guyot-Sionest Q, Larrieu C, Landrin V, Majorel G, Wittreck S, Woringe E, et  
1358 al. 2017. Risk factor analysis of equine strongyle resistance to anthelmintics. *Int J Parasitol Drugs*  
1359 *Drug Resist* 7:407–415.

1360 [Sallé G, Kornaś S, Basiaga M. 2018. Equine strongyle communities are constrained by horse sex and species  
1361 dispersal-fecundity trade-off. \*Parasites & Vectors\* 11:279.](#)

1362 Sallé G, Doyle SR, Cortet J, Cabaret J, Berriman M, Holroyd N, Cotton JA. 2019. The global diversity of  
1363 *Haemonchus contortus* is shaped by human intervention and climate. *Nat Commun* 10:4811.

1364 Sallé G, Guillot J, Tapprest J, Foucher N, Sevin C, Laugier C. 2020. Compilation of 29 years of postmortem  
1365 examinations identifies major shifts in equine parasite prevalence from 2000 onwards. *Int J Parasitol*  
1366 50:125–132.

1367 Sargison N, Chambers A, Chaudhry U, Costa Júnior L, Doyle SR, Ehimiyein A, Evans M, Jennings A, Kelly R,  
1368 Sargison F, et al. 2022. Faecal egg counts and nemabiome metabarcoding highlight the genomic  
1369 complexity of equine cyathostomin communities and provide insight into their dynamics in a Scottish  
1370 native pony herd. *Int J Parasitol* 52:763–774.

1371 Scare JA, Lyons ET, Wielgus KM, Nielsen MK. 2018. Combination deworming for the control of double-  
1372 resistant cyathostomin parasites – short and long term consequences. *Veterinary Parasitology*  
1373 251:112–118.

1374 Schwarz EM, Hu Y, Antoshechkin I, Miller MM, Sternberg PW, Aroian RV. 2015. The genome and  
1375 transcriptome of the zoonotic hookworm *Ancylostoma ceylanicum* identify infection-specific gene  
1376 families. *Nat Genet* 47:416–422.

1377 Seppay M, Manni M, Zdobnov EM. 2019. BUSCO: Assessing Genome Assembly and Annotation  
1378 Completeness. *Methods Mol Biol* 1962:227–245.

1379 Sieburth D, Ch’ng Q, Dybbs M, Tavazoie M, Kennedy S, Wang D, Dupuy D, Rual J-F, Hill DE, Vidal M, et al.  
1380 2005. Systematic analysis of genes required for synapse structure and function. *Nature* 436:510–517.

1381 [Silva AV, Costa HM, Santos HA, Carvalho RO. 1999. Cyathostominae \(Nematoda\) parasites of \*Equus caballus\*  
1382 in some Brazilian states. \*Vet Parasitology\* 85:15-21.](#)

1383 Sleight JN. 2010. Functional analysis of nematode nicotinic receptors. *Bioscience Horizons* 3:29–39.

1384 Tarailo-Graovac M, Chen N. 2009. Using RepeatMasker to identify repetitive elements in genomic sequences.  
1385 *Curr Protoc Bioinformatics* Chapter 4:4.10.1-4.10.14.

1386 The cyathostomin genomics consortium. 2023. Cyathostomin genomics. Available from:  
1387 <https://doi.org/10.57745/1FB35D>

1388 Tombak KJ, Hansen CB, Kinsella JM, Pansu J, Pringle RM, Rubenstein DI. 2021. The gastrointestinal nematodes  
1389 of plains and Grevy’s zebras: Phylogenetic relationships and host specificity. *International Journal for*  
1390 *Parasitology: Parasites and Wildlife* 16:228–235.

1391 Tydén E, Enemark HL, Franko MA, Höglund J, Osterman-Lind E. 2019. Prevalence of *Strongylus vulgaris* in  
1392 horses after ten years of prescription usage of anthelmintics in Sweden. *Veterinary Parasitology: X*  
1393 2:100013.

1394 Uliano-Silva M, Gabriel R. N. Ferreira J, Krashennikova K, Darwin Tree of Life Consortium, Formenti G,  
1395 Abueg L, Torrance J, Myers EW, Durbin R, Blaxter M, et al. 2022. MitoHiFi: a python pipeline for  
1396 mitochondrial genome assembly from PacBio High Fidelity reads. *Bioinformatics* Available from:

Formatted: Font: Italic

Field Code Changed

Field Code Changed

Deleted: dipersal-fecundity

Formatted: Font: Italic

Deleted: 29

Formatted: Font: Italic

Formatted: Font: Italic

1399 <http://biorxiv.org/lookup/doi/10.1101/2022.12.23.521667>  
1400 Von Samson-Himmelstjerna G, Thompson RA, Krücken J, Grant W, Bowman DD, Schnyder M, Deplazes P.  
1401 2021. Spread of anthelmintic resistance in intestinal helminths of dogs and cats is currently less  
1402 pronounced than in ruminants and horses – Yet it is of major concern. *International Journal for*  
1403 *Parasitology: Drugs and Drug Resistance* 17:36–45.  
1404 Wang C, Torgerson PR, Kaplan RM, George MM, Furrer R. 2018. Modelling anthelmintic resistance by  
1405 extending eggCounts package to allow individual efficacy. *Int J Parasitol Drugs Drug Resist* 8:386–  
1406 393.  
1407 Welz C, Kruger N, Schniederjans M, Miltsch SM, Krucken J, Guest M, Holden-Dye L, Harder A, von Samson-  
1408 Himmelstjerna G. 2011. SLO-1-channels of parasitic nematodes reconstitute locomotor behaviour  
1409 and emodepside sensitivity in *Caenorhabditis elegans slo-1* loss of function mutants. *PLoS Pathog*  
1410 7:e1001330.  
1411 Wingett SW, Andrews S. 2018. FastQ Screen: A tool for multi-genome mapping and quality control. *F1000Res*  
1412 7:1338.  
1413 Zhang Y, Park C, Bennett C, Thornton M, Kim D. 2021. Rapid and accurate alignment of nucleotide conversion  
1414 sequencing reads with HISAT-3N. *Genome Res.* 31:1290–1295.  
1415  
1416

Formatted: Font: Italic

